Article

Silent mutations reveal therapeutic vulnerability in RAS Q61 cancers

https://doi.org/10.1038/s41586-022-04451-4

Received: 24 November 2020

Accepted: 20 January 2022

Published online: 02 March 2022

Check for updates

Yoshihisa Kobayashi[1,2,3]✉, Chhayheng Chhoeu[4], Jiaqi Li[1], Kristin S. Price[5], Lesli A. Kiedrowski[5], Jamie L. Hutchins[5], Aaron I. Hardin[5], Zihan Wei[6], Fangxin Hong[6,7], Magda Bahcall[1,2], Prafulla C. Gokhale[4,8] & Pasi A. Jänne[1,2,8,9]✉

RAS family members are the most frequently mutated oncogenes in human cancers. Although KRAS(G12C)-specific inhibitors show clinical activity in patients with cancer[1–3], there are no direct inhibitors of NRAS, HRAS or non-G12C KRAS variants. Here we uncover the requirement of the silent *KRAS*^{G60G} mutation for cells to produce a functional KRAS(Q61K). In the absence of this G60G mutation in *KRAS*^{Q61K}, a cryptic splice donor site is formed, promoting alternative splicing and premature protein termination. A G60G silent mutation eliminates the splice donor site, yielding a functional KRAS(Q61K) variant. We detected a concordance of *KRAS*^{Q61K} and a G60G/A59A silent mutation in three independent pan-cancer cohorts. The region around *RAS* Q61 is enriched in exonic splicing enhancer (ESE) motifs and we designed mutant-specific oligonucleotides to interfere with ESE-mediated splicing, rendering the RAS(Q61) protein non-functional in a mutant-selective manner. The induction of aberrant splicing by antisense oligonucleotides demonstrated therapeutic effects in vitro and in vivo. By studying the splicing necessary for a functional KRAS(Q61K), we uncover a mutant-selective treatment strategy for *RAS*^{Q61} cancer and expose a mutant-specific vulnerability, which could potentially be exploited for therapy in other genetic contexts.

The effects of non-synonymous mutations—which alter the amino acid sequence of a protein—have been extensively investigated for their potential to disrupt normal human biology, causing cancer, and have been successfully targeted with specific drugs[4–6]. By contrast, the clinical significance of synonymous (silent) mutations remains unknown, despite evidence that silent mutations affect splicing, RNA stability, RNA folding, translation or co-translational protein folding[7,8]. In general, the role of synonymous mutations in cancer aetiology has not been systematically studied, and thus silent mutations are for the most part disregarded as noise in clinical mutational analyses.

Mutations in the RAS family genes are found in up to 20% of cancers: *KRAS* in non-small cell lung cancer (NSCLC), colorectal cancer and pancreatic cancer; *NRAS* in melanoma, colon cancer and leukaemia; and *HRAS* in bladder, breast and thyroid cancers[9]. Activated RAS proteins stimulate the downstream mitogen-activated protein kinase (MAPK) pathway, including MEK and ERK. Somatic mutations in *RAS* increase GTP-bound RAS, aberrantly activating MAPK signalling.

The development of targeted therapies for *RAS*-mutant cancers has been complex. MEK inhibitors combined with chemotherapy in *KRAS*-mutant NSCLC have limited efficacy[10]. Combined use of a MEK inhibitor with receptor tyrosine kinase (RTK) inhibitors to prevent ERK re-activation has also been proposed but the toxicity and low efficacy of the MEK inhibitor—owing to the lack of mutant selectivity—remains a challenge[11–13]. Allosteric inhibitors targeting SHP2, a non-receptor protein tyrosine phosphatase that transduces signalling from receptor tyrosine kinases to promote the activation of RAS, are currently in clinical development[14]. RAS-targeted therapies involve use of KRAS(G12C)-specific covalent inhibitors that lock the protein in its inactive, GDP-bound state[1]. Clinical trials have demonstrated encouraging clinical activity of these compounds in patients with NSCLC[2,3,15]. Another promising approach is to target SOS1, a key guanine exchange factor for KRAS that binds and activates GDP-bound RAS proteins at their catalytic binding sites and in this way promotes exchange of GDP for GTP. However, KRAS(Q61) mutants, which lack intrinsic GTP hydrolysis activity[16,17], are not responsive to SOS1 inhibitors, warranting the development of alternative Q61X-selective therapeutic strategies.

G60G is required for functional KRAS(Q61K)

Acquired somatic mutations in *KRAS* (G12C, G12D, Q61K and A146T) and *BRAF* (V600E) drive resistance to epidermal growth factor receptor (EGFR) tyrosine kinase inhibitor osimertinib in *EGFR*-mutant lung cancers[18,19]. To model these events in vitro, we introduced mutations into *KRAS* or *BRAF* in the *EGFR*-mutant lung cancer cell line PC-9 using CRISPR–Cas9 homology-directed repair and selected for resistance-imparting clones. Osimertinib

[1]Department of Medical Oncology, Dana-Farber Cancer Institute, Boston, MA, USA. [2]Department of Medicine, Harvard Medical School, Boston, MA, USA. [3]Division of Molecular Pathology, National Cancer Center Research Institute, Tokyo, Japan. [4]Experimental Therapeutics Core, Dana-Farber Cancer Institute, Boston, MA, USA. [5]Department of Medical Affairs, Guardant Health, Redwood City, CA, USA. [6]Department of Data Science, Dana-Farber Cancer Institute, Boston, MA, USA. [7]Harvard T. H. Chan School of Public Health, Boston, MA, USA. [8]Belfer Center for Applied Cancer Science, Dana-Farber Cancer Institute, Boston, MA, USA. [9]Lowe Center for Thoracic Oncology, Dana-Farber Cancer Institute, Boston, MA, USA. ✉e-mail: yoshikob@ncc.go.jp; pasi_janne@dfci.harvard.edu

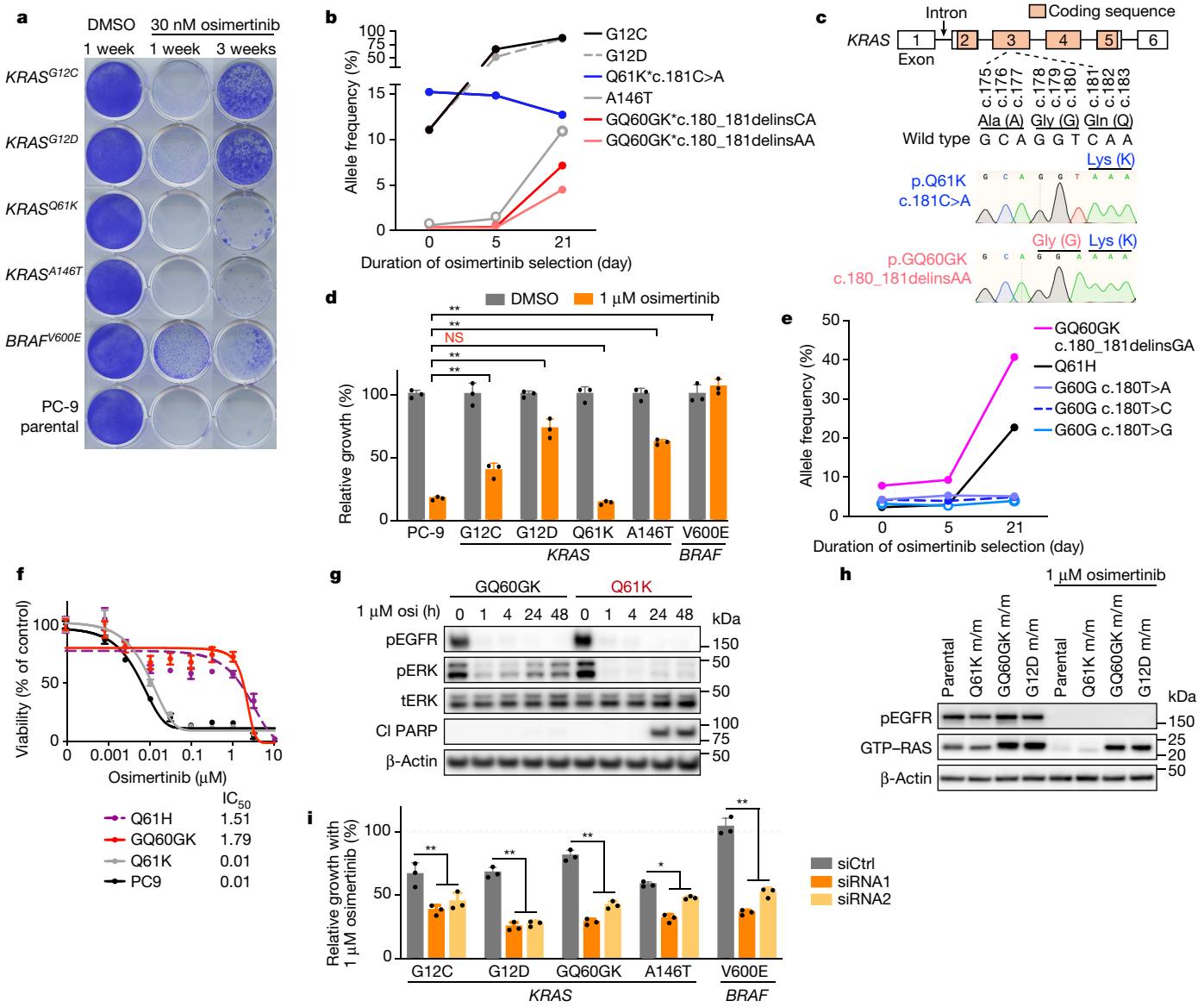

Fig. 1 | *KRAS*^{Q61K} imparts resistance to osimertinib only in the presence of a concurrent *KRAS*^{G60G} silent mutation. a, Colony formation assay for PC-9 cells of the indicated genotype following 1 or 3 weeks of treatment with osimertinib. **b**, Allele frequencies under osimertinib selection pressure, determined by NGS ($n = 1$). Asterisk indicates same donor template. **c**, Sequencing chromatograms of *KRAS* DNA derived from single clones. **d**, Cell viability assay for PC-9 cells of the indicated genotype after 72 h treatment with osimertinib ($n = 3$ biological replicates; mean ± s.d.; analysis of variance (ANOVA) followed by Dunnett's post hoc test). **e**, Allele frequencies by NGS under osimertinib treatment ($n = 1$). **f**, Cell viability assay for PC-9 cells with the indicated *KRAS* genotype after 72 h treatment ($n = 3$ biological replicates; mean ± s.d.). **g**, Western blot analyses following osimertinib treatment of PC-9 cells with the indicated *KRAS* genotype. pEGFR, phosphorylated EGFR; pERK, phosphorylated ERK; tERK, total ERK; cl PARP, cleaved PARP. **h**, RAS–GTP assay in *KRAS*-expressing PC-9 cells after 24 h treatment with or without 1 μM osimertinib. m, mutant allele. **i**, Growth of siRNA-resensitized PC-9 cells following knockdown of *KRAS* or *BRAF* genes with osimertinib treatment ($n = 3$ biological replicates; mean ± s.d.; Student's *t*-test). *$P < 0.05$, **$P < 0.01$. NS, not significant.

selectively enriched for cells harbouring different *KRAS* mutations or *BRAF*^{V600E} (Fig. 1a, Extended Data Fig. 1a). We monitored mutant allele frequencies over the course of drug selection using targeted next generation sequencing (NGS), and noted that although the allele frequencies of *KRAS* G12C, G12D and A146T mutations increased over time under osimertinib selection, the allele frequency of *KRAS*^{Q61K} decreased slightly (Fig. 1b). We noted that the allele frequencies of two other *KRAS*^{Q61K} alleles, both containing a concurrent silent mutation at G60, GQ60GK (c.180_181delinsCA or AA), increased sharply in response to drug treatment (Fig. 1b, c). The GQ60GK double mutants emerged from a CRISPR–Cas9 editing event that used the same donor template designed for the Q61K (c.181C>A) single mutant and are assumed to be the result of the error-prone non-homologous end joining repair. When tested for osimertinib sensitivity, single-cell clones of PC-9 cells harbouring *KRAS*^{Q61K} without this silent mutation did not impart resistance, and exhibited growth inhibition similar to that of parental cells. This was in stark contrast to the *KRAS* G12C, G12D, A146T and *BRAF* V600E clones, which were largely unaffected by 1 μM osimertinib treatment (Fig. 1d). Considering the 3 possible G60 mutant variants (c.180T>A, C, or G), we edited PC-9 cells using donor templates for *KRAS*^{GQ60GK} (c.180_181delinsGA), *KRAS*^{G60G} alone (c.180T>A, C, or G) and another non-synonymous mutation at codon 61, *KRAS*^{Q61H}. Following osimertinib treatment, the allele frequencies of GQ60GK (c.180_181delinsGA) and Q61H increased, but allele frequencies of G60G silent mutations alone remained unchanged (Fig. 1e).

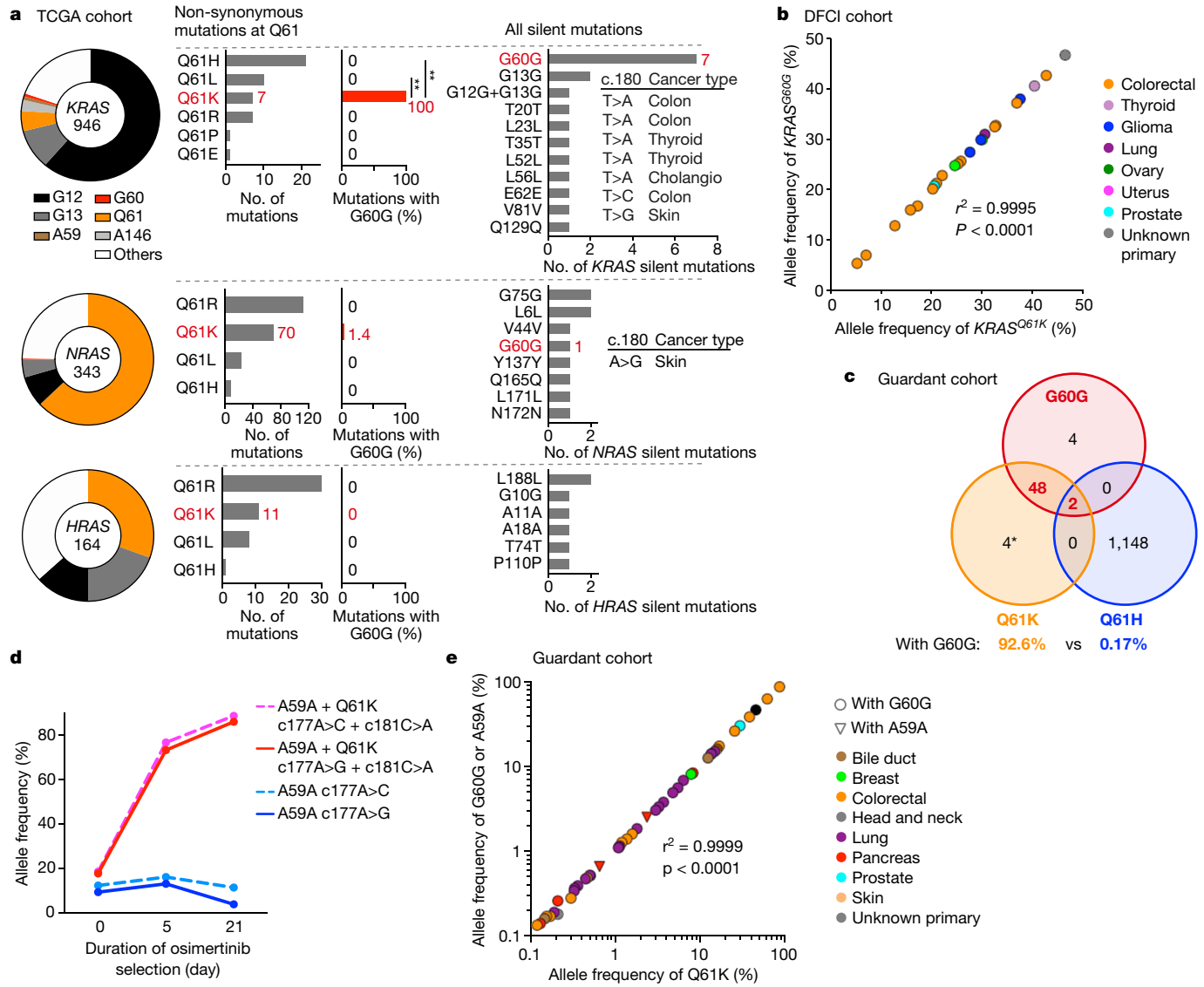

Fig. 2 | *KRAS*^{Q61K} co-occurs with the G60G silent mutation in three independent pan-cancer cohorts. a, Non-synonymous and silent mutations in *KRAS*, *NRAS* and *HRAS* genes obtained from the TCGA pan-cancer cohort. Pie charts include all non-synonymous and silent mutations in each gene. Non-synonymous mutations at Q61 and all silent mutations are shown in bar charts. The frequency of co-occurrence of activating non-synonymous Q61X and the G60G silent mutation was evaluated by Fisher's exact test. Background activating mutations that coexist with silent mutations are shown separately in Supplementary Table 1. **b**, Correlation between allele frequencies of *KRAS* Q61K and G60G in Dana-Farber Cancer Institute cohort evaluated by targeted NGS. Pearson's correlation coefficient is shown. **c**, Venn diagram showing the distribution of *KRAS* Q61K, G60G and Q61H mutations in the Guardant Health cohort, detected by targeted NGS using cell-free DNA. The co-occurrence of activating non-synonymous and G60G silent mutations was evaluated by Fisher's exact test. Asterisk indicates three cases with A59A. **d**, Allele frequencies evaluated by NGS in PC-9 models undergoing osimertinib treatment. **e**, The correlation between allele frequencies of *KRAS* Q61K and G60G/A59A in the Guardant Health cohort. Pearson's correlation coefficient is shown.

Heterozygous *KRAS* GQ60GK or Q61H mutations alone were sufficient to cause resistance to osimertinib in the PC-9 models (Fig. 1f, Extended Data Fig. 1b).

To examine the gain-of-function effect of the *KRAS* GQ60GK mutation, we evaluated its protein product and effect on downstream signalling. Following osimertinib treatment, persistent ERK1/2 activation was present in PC-9 cells expressing *KRAS*^{GQ60GK} but not in cells expressing *KRAS*^{Q61K} alone (Fig. 1g), confirming the uncoupling of EGFR inhibition from that of ERK1/2 in the double mutant only. In addition, *KRAS*^{GQ60GK} mutant cells exhibited robust RAS–GTP levels similar to those of *KRAS*^{G12D} cells at baseline, which were minimally affected by osimertinib (Fig. 1h). By contrast, RAS–GTP concentration decreased in osimertinib-treated *KRAS*^{Q61K} single-mutant and *KRAS* wild-type parental PC-9 cells. Reciprocally, short interfering RNA (siRNA)-mediated knockdown of *KRAS* or *BRAF* resensitized resistant PC-9 models to osimertinib, corroborating causality between *KRAS* or *BRAF* mutations and osimertinib resistance (Fig. 1i, Extended Data Fig. 1c). Collectively, our findings demonstrate a requirement of a silent mutation in *KRAS*^{G60G} for the biological function of KRAS(Q61K).

Concordance of *KRAS* G60G and Q61K

To establish the clinical significance of our finding, we surveyed The Cancer Genome Atlas (TCGA) data on mutants in *KRAS* and other RAS family members for the frequency of silent co-mutations. Q61 was the most frequently mutated codon in *NRAS* and *HRAS*, and the third most common mutation in *KRAS* (Fig. 2a, Supplementary Table 1). Silent mutations were found in 2–4% of all *RAS*

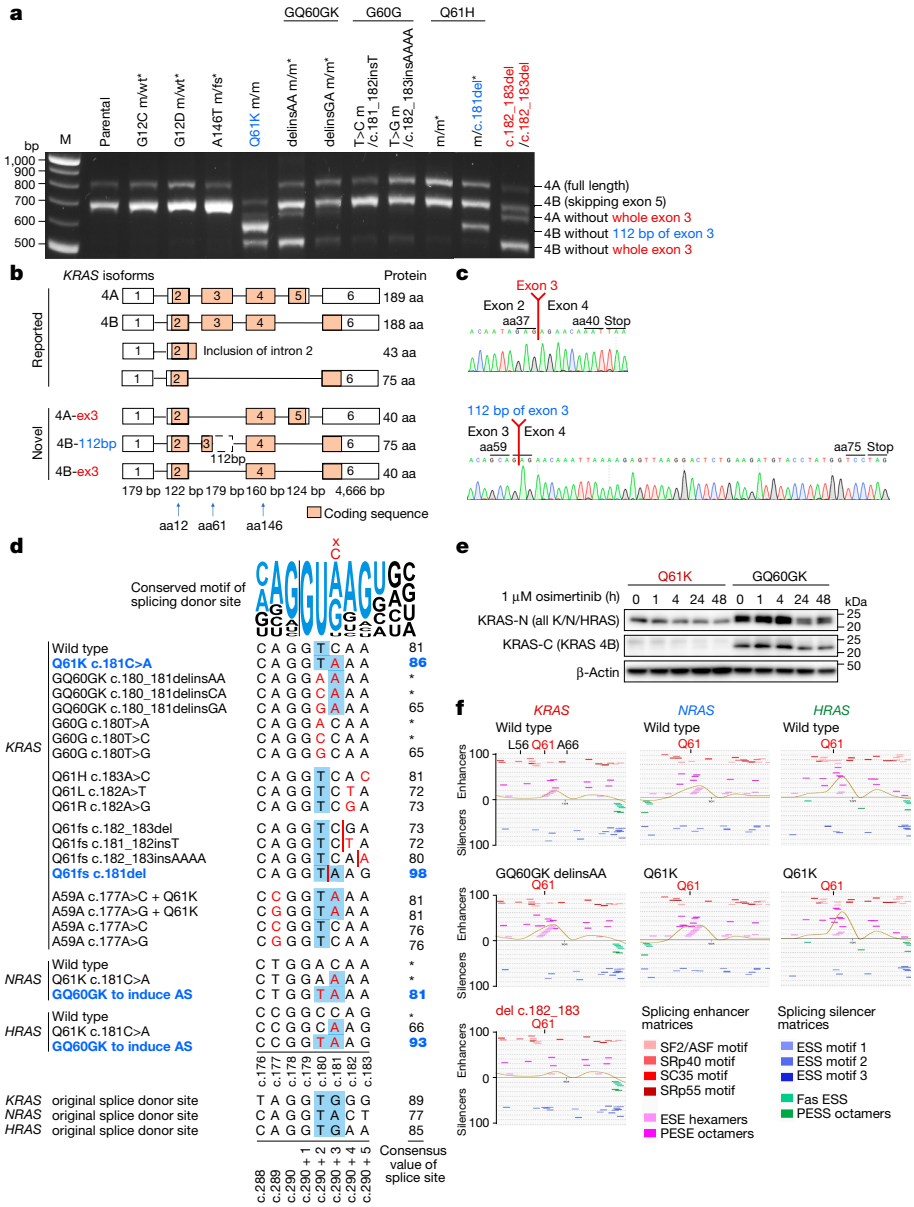

Fig. 3 | Silent mutation in *KRAS*^{G60G} is necessary for correct splicing of *KRAS*^{Q61K}. **a**, *KRAS*-specific PCR amplicons of cDNA, generated from CRISPR–Cas9-modified PC-9 clones. M, 100-bp marker; fs, frameshift; wt, wild type. Asterisk indicates clones growing under osimertinib selection pressure. **b**, Schemas of different *KRAS* isoforms shown in **a**. aa, amino acid. **c**, Sequencing chromatograms of *KRAS* cDNA derived from isoforms that lack 112 bp of exon 3 or the entire exon 3, which result in a subsequent frameshift and an early stop codon. **d**, Comparison of the conserved motif of splicing donor site and the DNA sequence of *KRAS*, *NRAS* and *HRAS* around Q61. Nucleotides at c.180 and c.181 that serve as putative cryptic splice donor sites are shaded in blue. Nucleotide changes, including deletions, are shown as red vertical bars. Consensus values of splice site were estimated by Human Splicing Finder. *KRAS* mutants with cryptic splice donor sites and their consensus values are shown in blue. AS, alternative splicing; asterisk indicates not reported. **e**, Western blot analysis in *KRAS*-expressing PC-9 models with antibodies targeting N-terminal or C-terminal epitopes of KRAS. **f**, ESE and ESS around *KRAS*, *NRAS* and *HRAS* Q61 were simulated using the Human Splicing Finder. Threshold values indicate the strength of each motif. Matrices for SR proteins including SF2/ASF, SRp40, SC35 and SRp55 were obtained from the ESE Finder tool. The RESCUE–ESE hexamers and the putative ESE (PESE) octamer are also shown. The relative strength of ESE and ESS octamers is denoted by a curved yellow line.

family-mutant cancers: 18 cases with mutations in *KRAS*, 10 with mutations in *NRAS*, and 7 with mutations in *HRAS*. Notably, however, all 7 cancers with *KRAS*^{Q61K} also contained *KRAS*^{G60G} (c.180T>A, C, or G) silent mutations. This co-occurrence was unique to *KRAS*^{Q61K} among *KRAS* mutations and G60G was only found once among 81 *NRAS*- or *HRAS*^{Q61K}-mutant cancers (Fig. 2a). To expand on this finding, we examined a pan-cancer cohort (n = 25,252) sequenced by targeted NGS at the Dana-Farber Cancer Institute and identified 23 cases with *KRAS*^{Q61K}, all of which contained a silent mutation at G60G (Fig. 2b). Of note, there was a high degree of concordance between the allele frequency of the mutations in *KRAS*^{Q61K} and *KRAS*^{G60G} (Fig. 2b, Supplementary Table 2).

Given the widespread use of liquid biopsies using plasma to detect genomic drivers and mechanisms of resistance in circulating tumour DNA and for monitoring the effect of treatment[20,21], we studied *KRAS* Q61K, G60G and Q61H cancers in the Guardant Health clinical cohort, analysed by targeted NGS (Guardant360). The co-occurrence of the *KRAS*^{G60G} silent mutations was significantly higher in *KRAS*^{Q61K} than in *KRAS*^{Q61H} cancers (Fig. 2c). Of the 54 cancers with *KRAS*^{Q61K}, 50 (93%) had *KRAS*^{G60G} silent mutations, compared with 2 out of 1,148 (0.17%) of

KRAS^{Q61H} cancers ($P < 0.0001$). Of note, both *KRAS*^{Q61H} cancers harbouring a *KRAS*^{G60G} silent mutation also contained a concomitant *KRAS*^{Q61K} mutation (Fig. 2c). In this cohort, three of the four *KRAS*^{Q61K} cancers that did not have a *KRAS*^{G60G} mutation contained a different silent mutation, *KRAS*^{A59A} (c.177A>A or G). Interrogating the functional significance of this mutation using the osimertinib selection assay of CRISPR-modified PC-9, we noted that the allele frequency of A59A alone did not increase under drug selection (Fig. 2d). However, in cells with a silent mutation in A59A in *cis* with Q61K, the allelic fraction increase mirrored that seen with GQ60GK (Figs. 1e, 2d). Data on allele frequencies of *KRAS* G60G and A59A were obtained in 45 cases with *KRAS*^{Q61K}; in the 45 cases, the allele frequencies of *KRAS*^{Q61K} correlated with *KRAS* G60G or A59A silent mutations (Fig. 2e). In the remaining 9 cases without available allele frequencies, the silent mutation in G60G and A59A was confirmed to be in *cis* with Q61K by manual review for analytic accuracy. Four cases had only *KRAS*^{G60G} silent mutations without *KRAS*^{Q61K} (Supplementary Table 3).

KRAS^{G60G} prevents aberrant Q61K splicing

To investigate the mechanism defining the reliance of functional *KRAS*^{Q61K} on silent mutations in *KRAS*^{G60G}, we amplified the cDNA of *KRAS* from CRISPR-modified PC-9 clones emerging in our screen, following osimertinib or control treatment (Fig. 3a). In addition to the two previously documented isoforms[22] 4A (full-length *KRAS*) and 4B (lacking exon 5) observed in parental PC-9 cells and clones expressing *KRAS* G12C, G12D, A146T, G60G and Q61H mutations, we identified two transcript isoforms in clones harbouring *KRAS* GQ60GK or Q61K. These isoforms are characterized by the absence of 112 bp in exon 3, or skipping of the entire exon 3 (Fig. 3a–c). Critically, neither isoform is expected to be translated to a functional KRAS(Q61K) owing to a frameshift introducing an early stop codon.

The sequence of wild-type *KRAS* around Q61 shows a high consensus with the conserved motif of a splice donor site[23], deviating only at c.181 (Fig. 3d). The mutation resulting in KRAS(Q61K) (c.181C>A) simultaneously introduces a putative cryptic splice donor site at that location, with a consensus value (86) that is equivalent to the canonical splice donor site between exon 3 and intron 3 (89), and thus could result in an aberrant splicing event producing either no protein or the non-functional Q61K variant observed in our screen. To test this hypothesis, we analysed the protein products of *KRAS*^{GQ60GK} and *KRAS*^{Q61K} by western blotting following an osimertinib challenge, using antibodies that bind either the N terminus (common to KRAS, NRAS and HRAS) or the C terminus (unique to KRAS 4B). The antibody directed against the N terminus detected RAS in both the *KRAS*^{Q61K} and *KRAS*^{GQ60GK} cells, the C-terminal antibody detected robust expression of KRAS(GQ60GK) but no (or minimal) expression of KRAS(Q61K) (Fig. 3e). Collectively, these data indicate that *KRAS*^{Q61K} alone cannot produce full-length KRAS protein that is competent to impart osimertinib resistance (Figs. 1h, 3e).

Another of our CRISPR-edited PC-9 clones contains a heterozygous deletion of c.181 along with Q61H (Fig. 3a). This single-base-pair deletion similarly introduces a cryptic splice site with a high consensus value (98), leading us to conclude that aberrant splicing at this site is responsible for deleting 112 bp of exon 3 in this isoform (Fig. 3a, d), creating a frameshift. Silent mutations at *KRAS* G60G (c.180T>A, C or G) disrupt the cryptic splice donor site introduced by the *KRAS*^{Q61K} mutation, as evidenced by its low consensus value relative to the conserved splice site (Fig. 3d). Other *KRAS*^{Q61X} variants such as Q61H/L/R do not generate a cryptic splice donor site because these mutations occur in c.182 or 183 (Fig. 3d). *KRAS*^{A59A} (c.177A>A or G) silent mutations (Fig. 2c), similar to *KRAS*^{G60G} silent mutations, decrease the splice site consensus values in *KRAS*^{Q61K} and thus produce a functional KRAS(Q61K) (Figs. 2d, 3d). In *NRAS* or *HRAS*, c.180 in the wild-type sequence is an A or C, and consequently *NRAS* or *HRAS* Q61K mutations do not introduce a cryptic splice donor site. These findings are consistent with the clinical data showing that the G60G silent mutation occurs uniquely in the *KRAS*^{Q61K} background (Fig. 2a). We, however, speculate that introducing silent mutations exogenously into *NRAS*^{Q61K} or *HRAS*^{Q61K} would also render these proteins non-functional—a silent mutation at G60G (A>T or C>T) in *NRAS* or *HRAS* Q61K would create a hypothetical cryptic splice donor site predicted to induce aberrant splicing (Fig. 3d).

We next examined the mechanism behind complete exon 3 exclusion, leading to premature termination (Fig. 2a, c). Using the Human Splicing Finder prediction software[24], we surveyed *KRAS* exon 3 for putative ESE and exonic splicing silencer (ESS) motifs and determined that the region around *KRAS* Q61K is enriched in ESE motifs (Fig. 3f). ESEs serve as a binding signal for specific serine/arginine-rich (SR) proteins and other splicing regulators that recruit the splicing machinery to weak splice sites flanking an exon and enhance exon inclusion[23]. Even a single nucleotide change can disrupt or introduce an ESE or ESS signal and promote aberrant splicing, including one that deletes an entire exon[25]. A case in point, a di-nucleotide deletion at *KRAS* c.182_183 substantially alters the putative ESE motif (Fig. 3f), leading to exon 3 exclusion (Fig. 3a). The skipping of the entire exon 3 was also observed in other clones harbouring mutations at *KRAS* Q61 (Extended Data Fig. 2a, b). A minority of cancers also have a natural proclivity to splice out the entire exon 3 at baseline (Extended Data Fig. 2c, Supplementary Table 4) although this occurs at a low (10%) frequency. Of note, ESE motifs are also found in *NRAS*^{Q61} and *HRAS*^{Q61} (Fig. 3f).

Taken together, we uncover a novel mechanism, whereby a silent mutation in G60G in the *KRAS*^{Q61K} context prevents aberrant splicing and is absolutely required to guarantee proper translation of this *KRAS* mutant. Our screen further exposes other vulnerabilities associated with mutations in the vicinity of *KRAS* Q61, including fatal alterations to endogenous ESE motifs, leading to aberrant splicing.

Therapeutic vulnerability of KRAS(GQ60GK)

We next applied the insights gained from studying the different *KRAS* mutants that affect splicing into potential therapeutic strategies. We hypothesized that antisense oligonucleotides designed against the ESE motifs in pre-mRNA of *KRAS*, *NRAS* or *HRAS* would compete for binding to these sites with the SR proteins, leading to a deleterious exclusion of the whole exon 3 and causing early termination. An alternative strategy to convert KRAS(GQ60GK) to the non-functional KRAS(Q61K) is to correct a *KRAS*^{G60G} silent mutation using CRISPR–Cas9 (Extended Data Fig. 3a–c). However, although technically achievable, this approach is unlikely to be clinically feasible in the near term, and we therefore focused on the antisense-oligonucleotide approach.

We used morpholino and DNA with phosphorothioate (PS) + 2′-*O*-methoxyethyl (2′MOE) modifications to generate antisense oligos (Extended Data Fig. 4a). Both types of antisense oligonucleotides are modified from natural nucleic acids to strongly and specifically bind to complementary target sites and are more stable in the presence of nucleases than DNA[26]. We designed mutant-selective morpholinos for *KRAS*, *NRAS* and *HRAS* Q61X, as well as control morpholinos with three mismatches to these sequences, taking into consideration the putative ESE sites and the potential for the oligonucleotide to self-dimerize (Extended Data Fig. 4b, Supplementary Table 5). Morpholino oligonucleotides against *HRAS*^{Q61X} were not able to cover ESEs around codon 57 and 58 as the oligonucleotides were predicted to self-dimerize and as such not effectively bind this region. The mean difference in predicted affinity (T_m) between morpholinos against the mutant or wild-type allele was 4.8 (1.8–9.3) °C (Supplementary Table 6). Morpholinos targeting *KRAS*^{GQ60GK} revealed up to a 9.3 °C T_m difference relative to the wild-type counterparts.

A genome-wide screen revealed that none of the 9 morpholines exhibited 100% homology against antisense off-target genes. When allowing for up to three mismatches, only mor-6 (three mismatches) had a

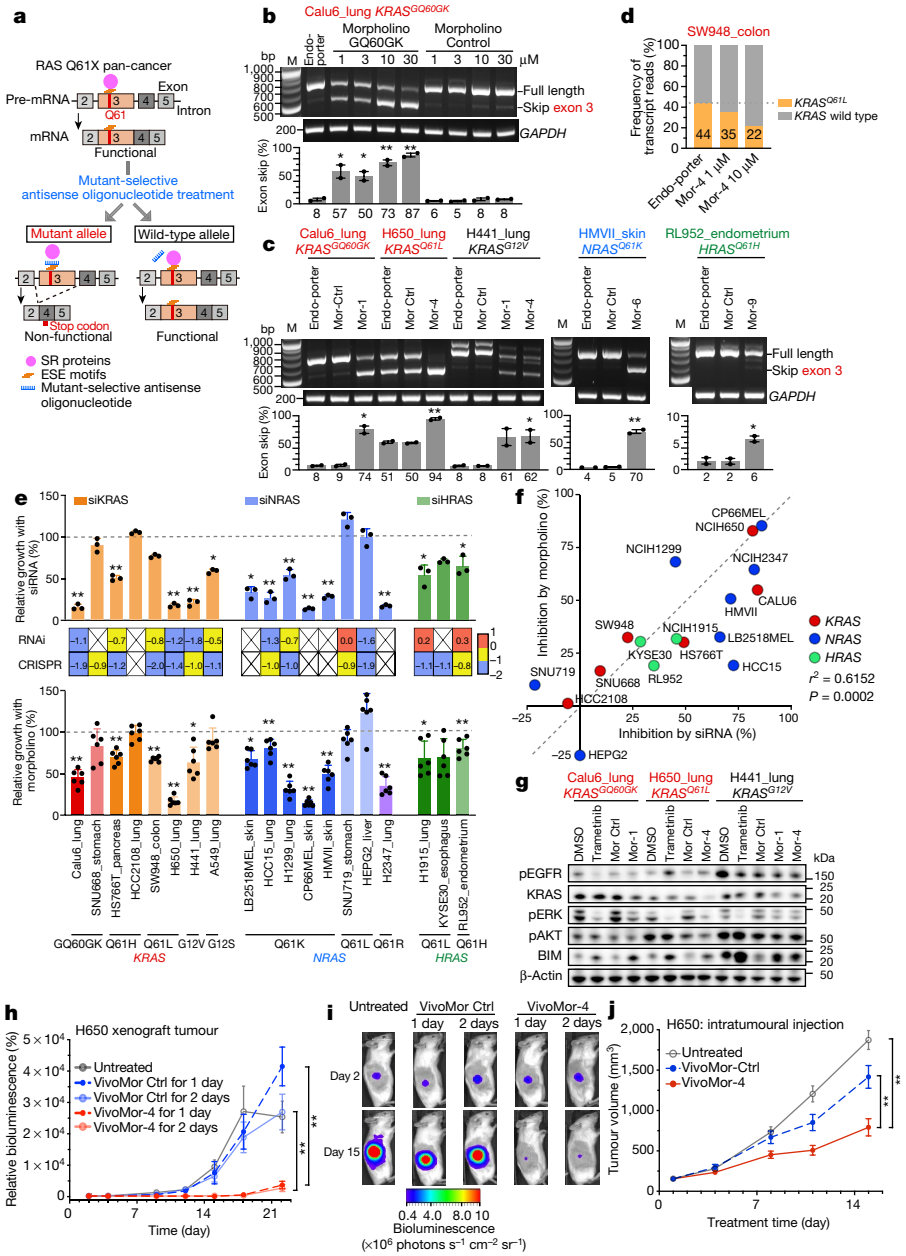

Fig. 4 | Antisense oligonucleotide induces aberrant splicing and therapeutic effects in vitro and in vivo. a, Antisense oligonucleotides hybridize to the ESE motifs in mutant but not in wild-type pre-mRNA and induce skipping of exon 3, resulting in premature termination. **b**, **c**, *KRAS*-specific PCR amplicons from cDNA of cells treated with different morpholino (Mor) concentrations (**b**) or 10 μM morpholino (**c**) for 48 h. The exon-skipping fraction is defined as skipped/(skipped + full-length) transcript ($n = 2$ biological replicates; mean ± s.e.m.; Student's *t*-test). Ctrl, control. **d**, Transcript frequencies of mutant versus wild-type in the intact full-length *KRAS* amplicon derived from SW948 cells treated with morpholino ($n = 1$). **e**, Relative RAS dependency and sensitivity to antisense oligonucleotides. Gene effect scores for dependency were obtained from Depmap, where a score of 0 is equivalent to a gene that is not essential and a score of −1 corresponds to the median of all common essential genes. Cells were treated with siRNA and 10 μM mutant-selective morpholino for 8 days ($n = 3$–6 biological replicates; mean ± s.d.; Student's *t*-test. **f**, Correlation of growth inhibition by siRNA and morpholino. Pearson's correlation coefficient is shown. **g**, Immunoblots of extracts from cells treated with 10 nM trametinib or 10 μM morpholino for 3 days. **h**, Luciferase-expressing H650 cells were pre-treated with 10 μM vivo-morpholino (vivoMor) in vitro for 1 or 2 days before injection into mice; xenograft tumours were then scanned twice per week ($n = 10$ per group; mean ± s.e.m.; Student's *t*-test and linear mixed growth models at day 22). **i**, Images of pre-treated H650 xenograft tumours. **j**, In vivo efficacy of daily intra-tumoral injection of morpholino on H650 xenograft tumours ($n = 10$ per group; mean ± s.e.m.; Student's *t*-test and linear mixed growth models at day 15).

potential off-target homology sequence, but its targets were located on the sense strand (and thus were unable to bind) or in non-coding regions (Supplementary Table 7a). Additionally, sequences trimmed by one nucleotide on both ends were evaluated to simulate binding of end-degraded morpholinos[27]. Genes within 3 mismatches showed a mean 10.5 (4.1–15.6) °C difference in the predicted binding affinity between on-target and potential off-target sites, and are thus unlikely to result in off-target binding (Supplementary Table 7b).

Selective antisense oligonucleotides would be predicted to induce aberrant splicing only in tumour cells, but not in normal cells lacking the Q61 mutation, potentially minimizing off-target toxicity (Fig.4a). Using this approach, we induced exon 3 skipping

in the *KRAS*^{GQ60GK} Calu6 lung cancer cell line, in a dose-dependent manner (Fig. 4b). The control oligonucleotide induced no exon 3 skipping. This observation extended to additional cancer cell lines harbouring *KRAS*, *NRAS* and *HRAS* Q61X mutations, which exhibited oligonucleotide-mediated mutant-selective exon 3 skipping (Fig. 4c). To assess the selectivity of the morpholino for the *KRAS* mutant over wild-type transcript, we had to determine the identity of the full-length pre-mRNA contributing to the exon 3 spliced mRNA following morpholino treatment. Since this information cannot be extracted from the exon 3-skipped cDNA sequence itself—the Q61-bearing exon 3 is spliced out—we focused our analysis on the composition of the full-length *KRAS* cDNA amplicon instead. We amplified *KRAS* cDNA generated from morpholino-treated SW948 cells using PCR, separated it by gel electrophoresis and used NGS to analyse the remaining full-length transcript to obtain the ratio of mutant versus wild-type *KRAS* pre-mRNA targeted by the morpholino. NGS analysis analogous to standard allele-frequency quantification revealed that mor-4 preferentially targeted the mutant *KRAS* pre-mRNA and decreased its fraction relative to the full-length transcript species in a dose-dependent manner from 44% to 22%, which directly supports the notion that morpholino treatment induces mutant-selective splicing (Fig. 4d, Extended Data Fig. 5). We next evaluated the effect of these oligonucleotides on cell growth. As not all *RAS* mutant cell lines depend on RAS signalling for their growth[28], we assessed *RAS* dependency of each of the Q61 mutant cell lines using *KRAS*-, *NRAS*- or *HRAS*-specific siRNAs, and compared our findings to published gene effect scores for dependency by RNA-mediated interference (RNAi) and CRISPR knockout obtained from Depmap (Fig. 4e). Cell lines that were dependent on *RAS* for their growth as determined by siRNA were also growth-inhibited following selective morpholino oligonucleotide treatment (Fig. 4e, Extended Data Fig. 6a). In aggregate, there was a significant concordance between growth inhibition by siRNA and that by morpholino oligonucleotide treatment (Fig. 4f). We also evaluated MEK inhibitor sensitivity in a panel of these cell lines using trametinib (Extended Data Fig. 6b). Of note, the *KRAS*^{Q61L} H650 lung cell line is highly resistant to trametinib but sensitive to antisense oligonucleotide (Extended Data Fig. 6b, c). Resistance to trametinib in H650 is the result of pEGFR reactivation and sustained pAKT signalling, whereas antisense oligonucleotide treatment inhibited both pERK and pAKT without this feedback (Fig. 4g, Extended Data Fig. 6d). We further confirmed that the expression of ERK signature genes[29] in *KRAS* mutant cells was reduced after treatment with antisense oligonucleotides (Extended Data Fig. 6e). In models not sensitive to single agent morpholino treatment, some were sensitive to EGFR inhibitor monotherapy or the combination of an EGFR inhibitor and the morpholino (Extended Data Fig. 6f, g). We next studied the morpholino treatment strategy in vivo. We initially used morpholino fused with a carrier. However, no exon 3 skipping was seen in tumours with intravenous administration due to the poor drug delivery (data not shown). We circumvented the issue by employing a pre-treatment strategy (Extended Data Fig. 7a). When piloted in vitro, morpholino oligonucleotide pre-treatment for 1 to 4 days followed by wash-out potently inhibited cell growth (Extended Data Fig. 7b). We subsequently pre-treated H650 lung cancer cells for one or two days with either the mutant-selective or control vivo-morpholino before injecting the same number of viable cells from each treatment condition in vivo. The control vivo-morpholino treated cells grew at a similar rate to the untreated cells (Fig. 4h, i). However, there was a significant decrease in growth in vivo as measured by either luciferase or tumour volume in the cells treated with the mutant-selective morpholino (Fig. 4h, i, Extended Data Fig. 7c). Furthermore, intra-tumoural injection of vivo-morpholinos demonstrated induction of *KRAS* exon 3 skipping (Extended Data Fig. 8a–d), and a significant reduction in tumour size compared to control or untreated tumours (Fig. 4j). In a second *KRAS*^{GQ60GK}-mutant xenograft model (Calu6), treatment was also effective when the pre-treatment approach was used (Extended Data Fig. 9a, b), and led to a positive efficacy trend, albeit not statistically significant, through the intra-tumoural injection approach (Extended Data Fig. 9c, d). We further evaluated the efficacy of a second type of antisense oligonucleotide technology, PS + 2′MOE oligonucleotides and observed that they achieved mutant-selective exon skipping and growth inhibition in vitro at much lower concentrations compared with morpholino oligonucleotides (Extended Data Fig. 10a–f, Supplementary Tables 8, 9).

Discussion

Here we uncover an essential role of silent mutations in splicing and production of a functional oncogene. Our *RAS*-directed CRISPR-editing and drug-pressure screen show the effects of silent mutations, namely *KRAS*^{G60G}, on splicing and translation of a functional KRAS(Q61K). Previous studies using conventional extrinsic overexpression of the coding sequences alone could not have identified the biological necessity of the silent mutation because the cDNA of an already-spliced transcript is used in such models. Our CRISPR models enabled the evaluation of splicing events and manual review of *KRAS*^{G60G} silent mutations in clinical samples, uncovering novel biology of *KRAS*^{G60G} which had previously not been appreciated. A functional KRAS(Q61K) requires a dinucleotide change, and thus may explain the rarity of this mutation in patients (0.7% of all *KRAS* mutations) in contrast to *NRAS*^{Q61K} (20% of all *NRAS* mutations) or *HRAS*^{Q61K} (7% of all *HRAS*) mutations, which are oncogenic owing to a single-base-pair substitution. Although the existence of *KRAS*^{G60G} silent mutations had been detected using a computational algorithm from a repository of cancer genomic data, their functional significance was previously unknown[30]. We identified two different splicing vulnerabilities that can be exploited therapeutically: a cryptic splice donor site in *KRAS*^{GQ60GK} cancers and ESE motifs in *KRAS*, *NRAS* and *HRAS* Q61X-mutant cancers. We provided a proof of concept showing that the induction of aberrant exon 3 exclusion in a mutant-selective manner using an antisense oligonucleotide approach produces non-functional RAS mutant protein and leads to tumour cell growth inhibition in vitro and in vivo. So far, only KRAS(G12C) has been directly therapeutically targeted but our findings also open the possibility for direct inhibition of RAS Q61X cancers.

Treatments for Duchenne muscular dystrophy using splice-modulating morpholinos and for spinal muscular atrophy using antisense oligonucleotide with PS + 2′MOE have been approved as therapies by the US Food and Drug Administration, supporting the potential clinical feasibility of our RAS Q61X-directed antisense oligonucleotide approach. Unlike previous antisense strategies targeting *STAT3* or *KRAS*, our strategy for targeting RAS Q61X is mutant-selective and thus should result in a wider therapeutic index and less toxicity in normal tissues[31,32]. As not all *KRAS*-mutant tumours are dependent on RAS, but also on other signals including EGFR[33], and targeting *KRAS*^{G12C} achieved responses in only a subset of such tumours[15], the correlation between the efficacy of our morpholino and RAS dependency further supports the on-target effects of this strategy. However, given the modest efficacy especially in our in vivo study, definitive proof will need to come from further testing in vivo and from clinical trials. Currently, toxicity and organ-specific in vivo delivery of both morpholinos and PS + 2′MOE antisense oligonucleotides are major limitations, and further optimization of chemical modifications, including conjugation to cell-penetrating short peptides[34,35], encapsulation and viral delivery is warranted[36].

Our findings provide new insights into the biological role of silent mutations in oncogenes and their great potential to be translated into novel therapies. The applicability of this strategy may extend to other genes on the basis of comprehensive analyses of silent mutations[37].

Further development of DNA-editing technologies may eventually enable direct editing of *KRAS*^{G60G} silent mutations to induce aberrant splicing in *KRAS*^{Q61K} cancers, abolishing their oncogenic capacity.

Online content

Any methods, additional references, Nature Research reporting summaries, source data, extended data, supplementary information, acknowledgements, peer review information; details of author contributions and competing interests; and statements of data and code availability are available at https://doi.org/10.1038/s41586-022-04451-4.

1. Ostrem, J. M., Peters, U., Sos, M. L., Wells, J. A. & Shokat, K. M. K-Ras(G12C) inhibitors allosterically control GTP affinity and effector interactions. *Nature* **503**, 548–551 (2013).
2. Canon, J. et al. The clinical KRAS(G12C) inhibitor AMG 510 drives anti-tumour immunity. *Nature* **575**, 217–223 (2019).
3. Hallin, J. et al. The KRAS(G12C) inhibitor MRTX849 provides insight toward therapeutic susceptibility of KRAS-mutant cancers in mouse models and patients. *Cancer Discov.* **10**, 54–71 (2020).
4. Middleton, G. et al. The National Lung Matrix Trial of personalized therapy in lung cancer. *Nature* **583**, 807–812 (2020).
5. Zehir, A. et al. Mutational landscape of metastatic cancer revealed from prospective clinical sequencing of 10,000 patients. *Nat. Med.* **23**, 703–713 (2017).
6. Ramalingam, S. S. et al. Overall survival with osimertinib in untreated, EGFR-mutated advanced NSCLC. *N. Engl. J. Med.* **382**, 41–50 (2020).
7. Diederichs, S. et al. The dark matter of the cancer genome: aberrations in regulatory elements, untranslated regions, splice sites, non-coding RNA and synonymous mutations. *EMBO Mol. Med.* **8**, 442–457 (2016).
8. Group, P. T. C. et al. Genomic basis for RNA alterations in cancer. *Nature* **578**, 129–136 (2020).
9. Consortium, A. P. G. AACR project GENIE: powering precision medicine through an international consortium. *Cancer Discov.* **7**, 818–831 (2017).
10. Janne, P. A. et al. Selumetinib plus docetaxel compared with docetaxel alone and progression-free survival in patients with *KRAS*-mutant advanced non-small cell lung cancer: the SELECT-1 randomized clinical trial. *JAMA* **317**, 1844–1853 (2017).
11. Kitai, H. et al. Epithelial-to-mesenchymal transition defines feedback activation of receptor tyrosine kinase signaling induced by MEK inhibition in *KRAS*-mutant lung cancer. *Cancer Discov.* **6**, 754–769 (2016).
12. Kruspig, B. et al. The ERBB network facilitates KRAS-driven lung tumorigenesis. *Sci. Transl. Med.* **10**, eaao2565 (2018).
13. Moll, H. P. et al. Afatinib restrains K-RAS-driven lung tumorigenesis. *Sci. Transl. Med.* **10**, eaao2301 (2018).
14. LaMarche, M. J. et al. Identification of TNO155, an allosteric SHP2 inhibitor for the treatment of cancer. *J. Med. Chem.* **63**, 13578–13594 (2020).
15. Hong, D. S. et al. KRAS(G12C) inhibition with sotorasib in advanced solid tumors. *N. Engl. J. Med.* **383**, 1207–1217 (2020).
16. Hunter, J. C. et al. Biochemical and structural analysis of common cancer-associated KRAS mutations. *Mol. Cancer Res.* **13**, 1325–1335 (2015).
17. Zhou, Z. W. et al. KRASQ61H preferentially signals through MAPK in a RAF dimer-dependent manner in non-small cell lung cancer. *Cancer Res.* **80**, 3719–3731 (2020).
18. Oxnard, G. R. et al. Assessment of resistance mechanisms and clinical implications in patients with EGFR T790M-positive lung cancer and acquired resistance to osimertinib. *JAMA Oncol.* **4**, 1527–1534 (2018).
19. Ramalingam, S. S. et al. Mechanisms of acquired resistance to first-line osimertinib: preliminary data from the phase III FLAURA study. *Ann. Oncol* **29**, VIII740 (2018).
20. Reinert, T. et al. Analysis of plasma cell-free DNA by ultradeep sequencing in patients with stages I to III colorectal cancer. *JAMA Oncol.* **5**, 1124–1131 (2019).
21. Chabon, J. J. et al. Integrating genomic features for non-invasive early lung cancer detection. *Nature* **580**, 245–251 (2020).
22. Amendola, C. R. et al. KRAS4A directly regulates hexokinase 1. *Nature* **576**, 482–486 (2019).
23. Cartegni, L., Chew, S. L. & Krainer, A. R. Listening to silence and understanding nonsense: exonic mutations that affect splicing. *Nat. Rev. Genet.* **3**, 285–298 (2002).
24. Desmet, F. O. et al. Human Splicing Finder: an online bioinformatics tool to predict splicing signals. *Nucleic Acids Res.* **37**, e67 (2009).
25. McVety, S., Li, L., Gordon, P. H., Chong, G. & Foulkes, W. D. Disruption of an exon splicing enhancer in exon 3 of MLH1 is the cause of HNPCC in a Quebec family. *J. Med. Genet.* **43**, 153–156 (2006).
26. Khvorova, A. & Watts, J. K. The chemical evolution of oligonucleotide therapies of clinical utility. *Nat. Biotechnol.* **35**, 238–248 (2017).
27. Kim, J. et al. Patient-customized oligonucleotide therapy for a rare genetic disease. *N. Engl. J. Med.* **381**, 1644–1652 (2019).
28. Janes, M. R. et al. Targeting KRAS mutant cancers with a covalent G12C-specific inhibitor. *Cell* **172**, 578–589.e517 (2018).
29. Brant, R. et al. Clinically viable gene expression assays with potential for predicting benefit from MEK inhibitors. *Clin. Cancer Res.* **23**, 1471–1480 (2017).
30. Chang, M. T. et al. Identifying recurrent mutations in cancer reveals widespread lineage diversity and mutational specificity. *Nat. Biotechnol.* **34**, 155–163 (2016).
31. Zammarchi, F. et al. Antitumorigenic potential of STAT3 alternative splicing modulation. *Proc. Natl Acad. Sci. USA* **108**, 17779–17784 (2011).
32. Ross, S. J. et al. Targeting *KRAS*-dependent tumors with AZD4785, a high-affinity therapeutic antisense oligonucleotide inhibitor of *KRAS*. *Sci. Transl. Med.* **9**, eaal5253 (2017).
33. Amodio, V. et al. EGFR blockade reverts resistance to KRAS^{G12C} inhibition in colorectal cancer. *Cancer Discov.* **10**, 1129–1139 (2020).
34. Klein, A. F. et al. Peptide-conjugated oligonucleotides evoke long-lasting myotonic dystrophy correction in patient-derived cells and mice. *J. Clin. Invest.* **129**, 4739–4744 (2019).
35. Boisguerin, P. et al. Delivery of therapeutic oligonucleotides with cell penetrating peptides. *Adv. Drug Deliv. Rev.* **87**, 52–67 (2015).
36. Imbert, M., Dias-Florencio, G. & Goyenvalle, A. Viral vector-mediated antisense therapy for genetic diseases. *Genes* **8**, 51 (2017).
37. Sharma, Y. et al. A pan-cancer analysis of synonymous mutations. *Nat. Commun.* **10**, 2569 (2019).

Publisher's note Springer Nature remains neutral with regard to jurisdictional claims in published maps and institutional affiliations.

© The Author(s), under exclusive licence to Springer Nature Limited 2022

Methods

Cell lines and drugs

Information on cell lines is listed in Supplementary Table 10. All cell lines were periodically tested negative for *Mycoplasma* using the Mycoplasma Plus PCR Primer Set (Agilent) throughout the study. Osimertinib, trametinib and afatinib were purchased from Selleck Chemicals. Cetuximab was purchased from Dana Farber Cancer Institute pharmacy.

Animals

Seven-week-old female NSG mice (for H650 xenograft model) and NCr nude mice (for Calu6 xenograft model) were purchased from The Jackson Laboratory. Animals were allowed to acclimatize for at least five days before initiation of the study. All in vivo studies were conducted at Dana-Farber Cancer Institute with the approval of the Institutional Animal Care and Use Committee in an AAALAC-accredited vivarium.

Genome editing using CRISPR–Cas9

To create *KRAS* or *BRAF* mutations in PC-9 cell lines, single guide RNAs (sgRNAs) and donor templates for homology-directed repair were designed using Deskgen (https://deskgen.com). CRISPR RNAs (crRNAs) (Integrated DNA Technologies) were hybridized with *trans*-activating crRNAs (tracrRNAs) to make 150 pmol sgRNAs, and then ribonucleoprotein complex was formed with 120 pmol Cas9 nuclease (Integrated DNA Technologies) in vitro. The reaction mixtures and 120 pmol donor templates were nucleofected into PC-9 cells (1×10^5 cells) suspended in 20 µl of SE solution (Integrated DNA Technologies) using Lonza 4D-Nucleofector (Lonza) with EN-138 mode. Cells were cultured in growth medium with 30 µM Alt-R HDR Enhancer (Integrated DNA Technologies) for 12 h. DNA was extracted from single clones using the DNeasy Mini kit (Qiagen) and mutations were confirmed by Sanger sequencing (Genewiz) or CRISPR sequencing at the Massachusetts General Hospital (MGH) DNA sequencing core. All sgRNAs, donor templates, and primers are listed in Supplementary Table 10.

Lentiviral transfection

Firefly luciferase lentivirus (1.5×10^6 colony-forming units (CFU), Karafast) was used to transduce cells (1.5×10^5 cells) in the presence of polybrene (5 µg ml^{-1}, Santa Cruz Biotechnology), followed by centrifugation at 1,200*g* for 90 min at 32 °C, and then cultured for 12 h at 37 °C. Luciferase-expressing cells were selected in 1 µg ml^{-1} puromycin (Thermo Fisher) for 5 days.

Colony formation assay and allele frequency evaluation

Bulk PC-9 cells edited to contain *KRAS* or *BRAF* mutations (1×10^5 cells) were seeded into 12-well plates and cultured with or without 30 nM osimertinib. After staining with 0.5% crystal violet in 25% methanol for 30 min, images were taken by EPSON perfection V750 pro. To evaluate allele frequency of specific mutant over time, DNA was extracted from bulk edited cells and submitted to CRISPR sequencing (MGH DNA core).

Gene knockdown by siRNA

Control siRNA or target-specific siRNA (final concentration of 10 nM, Life Technologies) and Lipofectamin RNAiMAX Transfection Reagent (final concentration of 0.3%, Thermo Fisher) were mixed in Opti-MEM (Gibco). After 10 min, the mixture was added into CRISPR-modified PC-9 cells with growth media. For growth-inhibition assay, cells were trypsinized 24 h after transfection, and cultured in 384-well plates for 24 h, then treated with osimertinib (Fig. 1i). For western blot analysis, samples were collected 48 h after transfection (Extended Data Fig. 1c). In experiments using RAS-mutant cell lines, control siRNA or indicated SMARTpool siRNA (final concentration of 25 nM, Dharmacon) and DharmaFECT1 or DharmaFECT2 (final concentration of 0.3%, Dharmacon) were mixed in Opti-MEM for 5 min, and then the reaction mixtures were added to cells in growth medium (Fig. 4e).

Cell growth inhibition assay

Parental or CRISPR-modified PC-9 cells (1×10^3 cells) were plated in 384-well plates. After 24 h, cells were treated with drugs at the indicated concentrations for 72 h. Endpoint cell viability assays were performed using Cell Titer Glo (Promega) and read by FLUOstar Omega. RAS-mutant cell lines (2×10^3 cells) were seeded in 384-well ultra-low-attachment plates as suspension cells and evaluated using 3D-Cell Titer Glo (Promega). *RAS* mutant cells were treated with trametinib for 3 days and with antisense oligonucleotides or siRNA for 8 days.

RAS isoforms

RNA was extracted using the RNeasy Mini kit (Qiagen) and cDNA was synthesized using the QuantiTect Reverse Transcription Kit (Qiagen). Isoforms were amplified using gene-specific-primers (Supplementary Table 10) and amplicons were resolved on a 2% agarose gel and scanned by Bio-Rad Universal Hood II Gel Documentation System with CFW-1312M camera. Isoforms were characterized by Sanger sequencing and shown using SnapGene 4.1.9.

Quantitative RT–PCR

The quantitative PCR reactions were set up in 20 µl using TaqMan Gene Expression Master Mix (Thermo Fisher) including 1 µl of 1:5 diluted cDNA synthesized from 1 µg RNA. The reactions were run in StepOne Plus Real-time PCR System (Applied Biosystems). Expression levels of target genes were normalized to those of GUSB housekeeping gene in each sample. Primers and probes were designed to target exon 1 to 2 of normal *KRAS* isoform and isoform with skipping 112 bp of exon 3 (Supplementary Table 10).

Antibodies and western blot analysis

Cells were lysed with RIPA buffer (Boston Bioproducts) supplemented with cOmplete Mini EDTA-free Protease inhibitor cocktail (Roche) and PhoSTOP phosphatase inhibitor cocktail (Roche). The total cell lysate (20 µg) was subjected to SDS polyacrylamide gel electrophoresis and transferred to Immobilon-P polyvinylidene difluoride membranes (Bio-Rad Laboratories). Antibodies are listed in Supplementary Table 10. Membraned were scanned by Amersham Imager 600 and analysed using ImageQuant TL1D v8.2. RAS-GTP was evaluated using the Active Ras Detection Kit (8821, Cell Signaling Technology). Cells were cultured with media containing 0.1% FBS with or without 1 µM osimertinib for 24 h, and 80 µg of GST–Raf1–RBD and 500 µg of protein lysates were used according to the manufacturer's instructions.

Simulating consensus value of splice site

Consensus values of splice site were estimated by Human Splicing Finder v3.1[24]. To evaluate distribution of ESE and ESS sites around *KRAS*, *NRAS* and *HRAS* Q61, wild-type and mutant sequences were simulated using the same Human Splicing Finder. For the purpose of designing antisense oligonucleotides, the locations of ESEs were also simulated using ESE finder 3.0[38,39] to be validated by independent algorisms. Threshold values indicate the strength of each motif. Matrices for SR proteins including SF2/ASF, SRp40, SC35 and SRp55 were obtained from the ESE Finder tool. The RESCUE-ESE hexamers[40] and the putative octamer ESE[41] are also shown.

Designing antisense oligonucleotides

Mutant-selective morpholino, vivo-morpholino (Gene Tools) and DNA with full PS + 2′MOE modification (Integrated DNA Technologies) were designed against the region of ESE motifs simulated by Human Splicing Finder and ESE finder, and self-dimerization potential was estimated using Oligo Analyzer (https://www.idtdna.com/calc/analyzer/).

Universal control 20-nt antisense oligonucleotides were designed with 3 mismatches relative to the wild-type sequence around *KRAS*, *NRAS* and *HRAS* Q61.

Binding affinity of morpholinos with mutant or wild-type sequences

Predicted binding affinity of antisense oligonucleotides designed against mutant or wild-type sequences were calculated using the UNAFold Web Server with a setting of 50 mM Na, 1.2 mM Mg and oligonucleotide 0.25 μM (http://www.unafold.org/Dinamelt/applications/hybridization-of-two-different-strands-of-dna-or-rna.php).

Dependency score

Gene-effect scores for dependency, evaluated by RNAi and CRISPR knockout, were obtained from Depmap (https://depmap.org/portal/), where a score of 0 is equivalent to a gene that is not essential whereas a score of −1 corresponds to the median of all common essential genes.

Treatment with morpholino or antisense oligonucleotide with PS + 2′MOE in vitro

RAS-mutant cell lines in culture media were treated in suspension with indicated concentrations of morpholino and 3–6 μM endo-porter (Gene Tools). Duration of treatment was 2 days for RNA experiments, 3 days for western blot and 8 days for growth-inhibition assay based on previously published treatment protocols with *KRAS*-selective inhibitors against RAS-mutant cells[3]. In all experiments using full PS + 2′MOE antisense oligonucleotides, medium was enriched with Ca^{2+}. Ca^{2+} enrichment of medium potentiates the in vitro activity of multiple types of oligonucleotides and is more reflective of in vivo conditions than conventional transfection methods[42]. Duration of treatment was 2 days for RNA experiments, 6 days for western blot and 8 days (drug treatment refreshed on day 3) for growth-inhibition assay.

Pilot study of pre-treatment strategy using vivo-morpholino in vitro

Cells in suspension were treated with vivo-morpholinos without endo-porter in culture media containing 1% FBS, followed by morpholino oligonucleotide wash-out. Then, cells were seeded into ultra-low attachment plates and cultured with complete media for 8 days until 3D-Cell Titer Glo assay.

In vivo efficacy study

Luciferase-expressing H650 and Calu6 cell lines were pre-treated with control vivo-morpholino or targeting vivo-morpholino without endo-porter in culture medium containing 1% FBS for 1 or 2 days. After morpholino oligonucleotide wash-out, the same number of viable cells (5×10^6 cells) with 50% Matrigel (Fisher Scientific) was implanted subcutaneously in the right flank of the mice. The tumour burden was assessed by bioluminescent imaging beginning from day 2 using IVIS Spectrum (Perkin Elmer) at least twice weekly. Tumour volumes were also measured using calliper measurements at least twice weekly. Total bioluminescence was measured as photons s^{-1} cm^{-2} sr^{-1} and the tumour volumes were determined by using the formula volume = (length × width^2)/2. Body weights were measured twice weekly. For intra-tumoral injection experiments, 0.5 mM vivo-morpholino reconstituted in PBS were injected daily. Tumour samples were collected to evaluate pharmacodynamics at 4 h after day 7 of drug administration.

Clinical data

Non-synonymous and silent mutations in *KRAS*, *NRAS* and *HRAS* genes were obtained from The Cancer Genome Atlas (TCGA) pan-cancer cohort. Pan-cancer cohort (n = 25,252) evaluated by targeted NGS OncoPanel[43] at the Dana-Farber Cancer Institute was queried and de-identified $KRAS^{Q61K}$ and $KRAS^{G60G}$ data were extracted. We performed a retrospective review of the Guardant Health de-identified database to identify *KRAS* Q61K-, Q61H- and G60G-mutation-positive patients with advanced stage solid tumours who had cell-free DNA sequencing as part of standard clinical care between March 2014 and November 2019. Testing was performed in a Clinical Laboratory Improvement Amendments (CLIA)-certified, College of American Pathologists (CAP)-accredited, New York State Department of Health-approved clinical laboratory at Guardant Health. Analysis was completed under an Advarra Review Institution Review Board protocol for de-identified and limited datasets and did not require specific patient consent. Plasma was analysed per methods previously described[44]. We analysed all reported genomic alterations from this cohort and performed a manual sequencing review for a subset of identified samples.

Statistics and reproducibility

Mean values were assessed using unpaired two-tailed Student's *t*-test or ANOVA followed by Dunnett's post hoc test. The correlation was analysed by Pearson's correlation coefficient. The frequency of co-occurrence of activating non-synonymous Q61X and the G60G silent mutation was evaluated by Fisher's exact test. For in vivo studies, two-tailed Student's *t*-tests were used to compare the tumour volume or relative bioluminescence at the last experimental time point and linear mixed models with random slopes were applied to compare the growth rate between treatment groups. $^*P < 0.05$, $^{**}P < 0.01$. GraphPad Prism9 and SAS 9.4 were used for all statistical analyses. Each experiment was repeated twice with similar results. Statistical analysis was conducted on data from biologically independent experimental replicates.

Reporting summary

Further information on research design is available in the Nature Research Reporting Summary linked to this paper.

Data availability

FASTQ files from the Amplicon sequencing of *KRAS* are available from the Sequence Read Archive database under BioProject accession number PRJNA789849. Non-synonymous and silent mutations in *KRAS*, *NRAS* and *HRAS* genes were obtained from TCGA pan-cancer cohort (https://portal.gdc.cancer.gov). Data on exon 3 skipping at baseline in the TCGA cohort were obtained from TCGA SpliceSeq (https://bioinformatics.mdanderson.org/public-software/tcgaspliceseq/). Gene effect scores for dependency, evaluated by RNAi and CRISPR knockout, were obtained from Depmap (https://depmap.org/portal/). Source data are provided with this paper.

38. Cartegni, L., Wang, J., Zhu, Z., Zhang, M. Q. & Krainer, A. R. ESEfinder: A web resource to identify exonic splicing enhancers. *Nucleic Acids Res.* **31**, 3568–3571 (2003).
39. Smith, P. J. et al. An increased specificity score matrix for the prediction of SF2/ASF-specific exonic splicing enhancers. *Hum. Mol. Genet.* **15**, 2490–2508 (2006).
40. Fairbrother, W. G. et al. RESCUE-ESE identifies candidate exonic splicing enhancers in vertebrate exons. *Nucleic Acids Res.* **32**, W187–W190 (2004).
41. Zhang, X. H. & Chasin, L. A. Computational definition of sequence motifs governing constitutive exon splicing. *Genes Dev.* **18**, 1241–1250 (2004).
42. Hori, S.-i et al. Ca^{2+} enrichment in culture medium potentiates effect of oligonucleotides. *Nucleic Acids Res.* **43**, e128 (2015).
43. Garcia, E. P. et al. Validation of OncoPanel: a targeted next-generation sequencing assay for the detection of somatic variants in cancer. *Arch. Pathol. Lab. Med.* **141**, 751–758 (2017).
44. Odegaard, J. I. et al. Validation of a plasma-based comprehensive cancer genotyping assay utilizing orthogonal tissue- and plasma-based methodologies. *Clin. Cancer Res.* **24**, 3539–3549 (2018).

Acknowledgements Y.K. is supported in part by JSPS Overseas Research Fellowships, Uehara Memorial Foundation, SGH Foundation and Suzuken Memorial Foundation. P.A.J. is supported in part by the Cammarata Family Foundation Research Fund, the American Cancer Society Clinical Research Professor Grant (CRP-17-111-01-CDD), the Mark Foundation for Cancer Research (grant no. 19-029 MIA), the Mock Family Fund for Lung Cancer Research and the Goldstein Family Research Fund. We thank S. Obika and T. Nakayama for advice on antisense oligonucleotides; D. A. Barbie for helpful discussion; and E. F. Cohen for visualizing fastq data on *KRAS* transcript reads in IVG software.

Author contributions Y.K. conceptualized the study, collected data from TCGA and DFCI cohorts, designed antisense oligonucleotides, developed and executed in vitro experiments and

wrote the paper. C.C. executed in vivo studies. J.L. executed in vitro experiments. K.S.P., L.A.K., J.L.H. and A.I.H. collected data from the Guardant Health cohort. Z.W. and F.H. performed statistical analyses. M.B. executed in vitro experiments, interpreted data, and wrote the paper. P.C.G. supervised and analysed in vivo studies. P.A.J. conducted and supervised all experiments, interpreted data and wrote the paper. All authors reviewed and commented on the paper.

Competing interests P.A.J. reports consulting fees from AstraZeneca, Boehringer-Ingelheim, Pfizer, Roche/Genentech, Takeda Oncology, ACEA Biosciences, Eli Lilly and Company, Araxes Pharma, Ignyta, Mirati Therapeutics, Novartis, Loxo Oncology, Daiichi Sankyo, Sanofi Oncology, Voronoi, SFJ Pharmaceuticals, Silicon Therapeutics, Nuvalent, Esai, Bayer, Biocartis, Allorion Therapeutics, Accutar Biotech and AbbVie; receiving post-marketing royalties from DFCI owned intellectual property on EGFR mutations licensed to Lab Corp; sponsored research agreements with AstraZeneca, Daichi-Sankyo, PUMA, Boehringer Ingelheim, Eli Lilly and Company, Revolution Medicines and Astellas Pharmaceuticals; and stock ownership in Loxo Oncology and Gatekeeper Pharmaceuticals. K.S.P., L.A.K., J.L.H. and A.I.H. are employees and stockholders of Guardant Health. P.A.J. and Y.K. are inventors on a patent on the therapeutic use of mutant specific antisense oligonucleotides.

Additional information

Supplementary information The online version contains supplementary material available at https://doi.org/10.1038/s41586-022-04451-4.

Correspondence and requests for materials should be addressed to Yoshihisa Kobayashi or Pasi A. Jänne.

Peer review information *Nature* thanks the anonymous reviewers for their contribution to the peer review of this work.

Reprints and permissions information is available at http://www.nature.com/reprints.

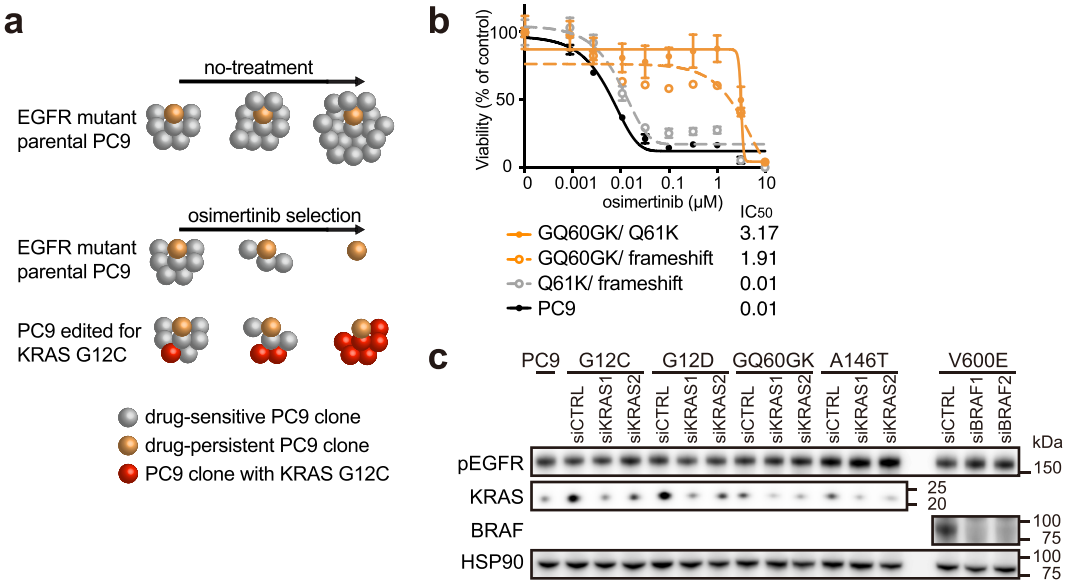

Extended Data Fig. 1 | CRISPR-Cas9 modified *EGFR* mutant PC-9 cells for evaluating oncogenicity of *KRAS* or *BRAF* mutations. a, A schema of selection with EGFR inhibitor osimertinib. Majority of parental *EGFR*-mutant PC-9 cells are sensitive to osimertinib with only a small fraction exhibiting intrinsic resistance. In bulk CRISPR-Cas9 modified PC-9 cells, osimertinib treatment can lead to an increase in the fraction of cells harboring a resistance mutation such as *KRAS* G12C. **b**, Cell viability assay of parental and CRISPR-Cas9 modified PC-9 cells after 72 h of osimertinib treatment. Each clone has heterozygous *KRAS* mutations: GQ60GK c.180_181delinsCA plus Q61K, GQ60GK c.180_181delinsGA plus frameshift, and Q61K plus frameshift (n = 3 biological replicates, mean ± s.d.). **c**, Knockdown of *KRAS* or *BRAF* in CRISPR-Cas9-modified PC-9 clones following 48 h of *KRAS* or *BRAF* specific siRNA treatment are shown by western blot analyses.

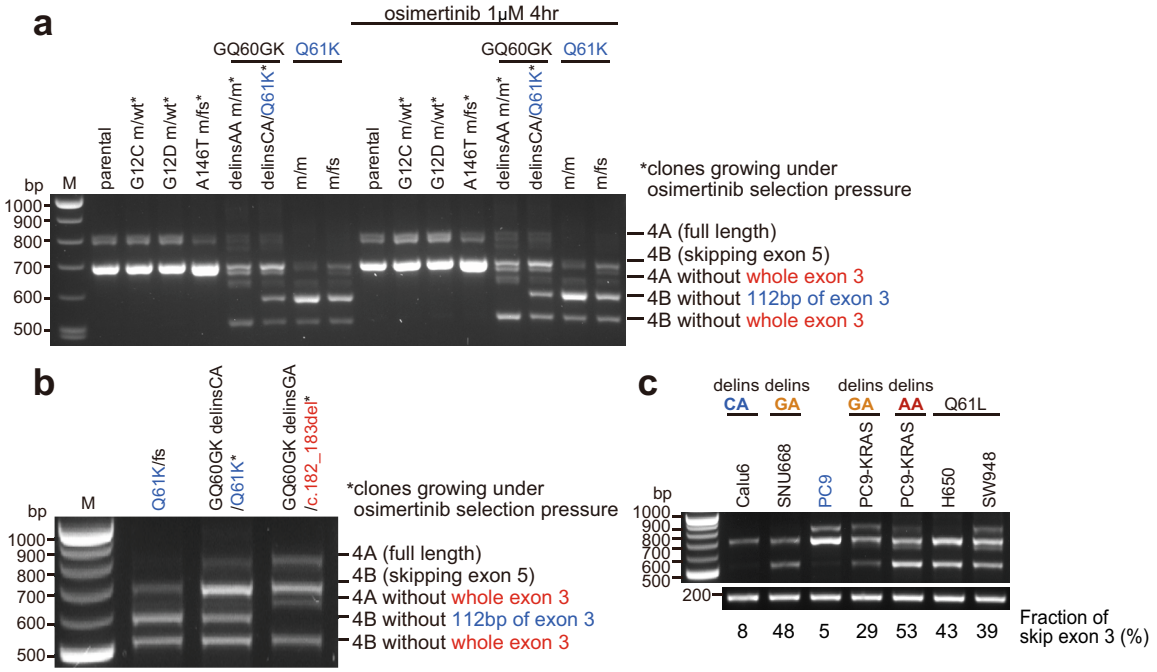

Extended Data Fig. 2 | Alternative splicing of *KRAS* in CRISPR-Cas9 modified PC-9 cells. a, Images of *KRAS*-specific PCR amplicons of cDNA, generated from CRISPR-Cas9 modified PC-9 clones expressing different *KRAS* mutations in the presence or absence of osimertinib given the influence of upstream EGFR signals. Heterozygosity or homozygosity of *KRAS* mutants is shown for each clone. M: 100 bp-marker, m: mutant, wt: wild-type, fs: frameshift. **b**, Images of *KRAS*-specific PCR amplicons of cDNA, generated from additional CRISPR-Cas9 modified PC-9 clones expressing different *KRAS* mutations. **c**, Images of *KRAS*-specific PCR amplicons of cDNA, generated from *KRAS* mutant cell lines and CRISPR-Cas9 modified PC-9 clones expressing different *KRAS* mutations.

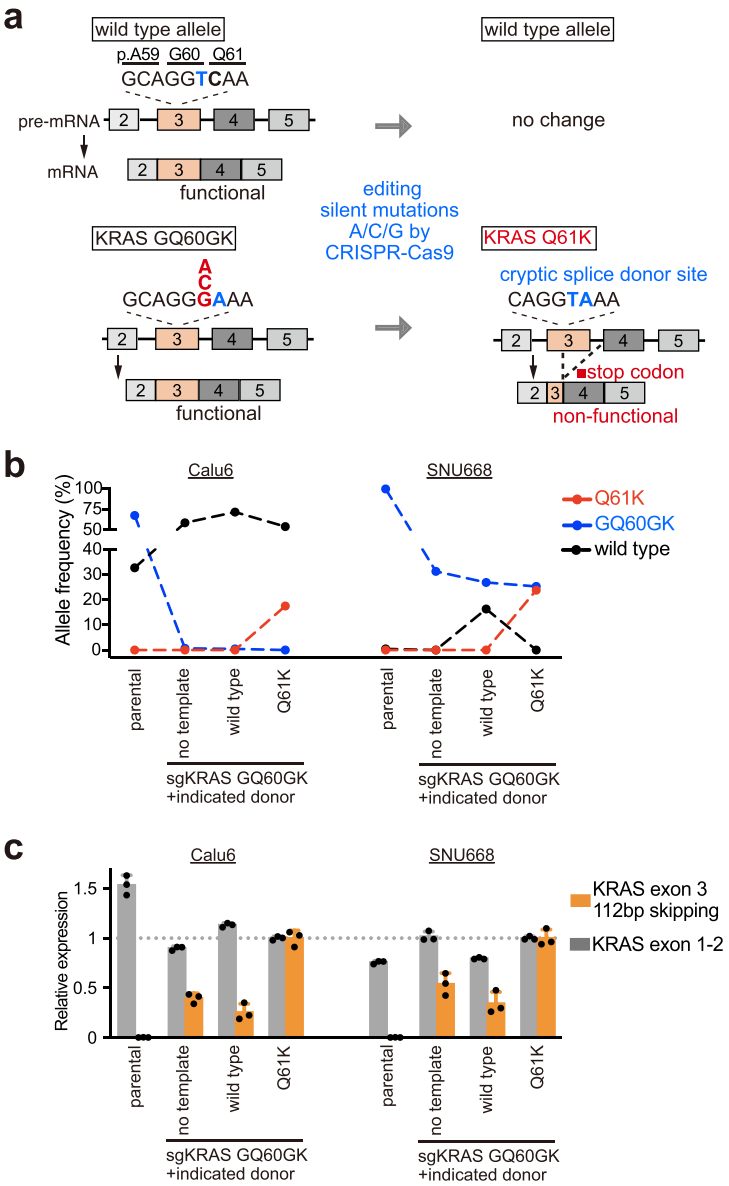

Extended Data Fig. 3 | A strategy to convert the original *KRAS* GQ60GK into the non-functional Q61K by editing silent mutations using CRISPR-Cas9. **a**, A schema of the proposed alternative treatment strategy using CRISPR-Cas9 editing with a mutant-specific sgRNA substituting the c.180 silent mutation with a cryptic splice donor nucleotide in order to promote exonic skipping leading to a premature STOP codon **b**, Allele frequencies of mutations, evaluated by next generation sequencing using DNA derived from bulk *KRAS* GQ60GK-mutant Calu6 and SNU668 cell lines, 48 h after CRISPR-Cas9 editing with indicated donor templates (n = 1). Allele frequency of original *KRAS* GQ60GK decreased by CRISPR editing with GQ60GK-specific sgRNA and allele frequency of non-functional Q61K increased only in the presence of donor template designed for Q61K. **c**, Relative expression of indicated *KRAS* isoforms, evaluated by qPCR in *KRAS* GQ60GK-mutant Calu6 and SNU668 cell lines, 48 h after CRISPR-Cas9 editing with indicated donor templates. Expression data are shown as relative to cell lines using Q61K template (n = 3 biological replicates, mean ± s.d.). Although it is difficult to capture clones successfully converted to non-functional Q61K due to their inability to grow, increased expression level of the KRAS isoform skipping 112 bp was confirmed in the remaining cells 2 days after CRISPR-editing.

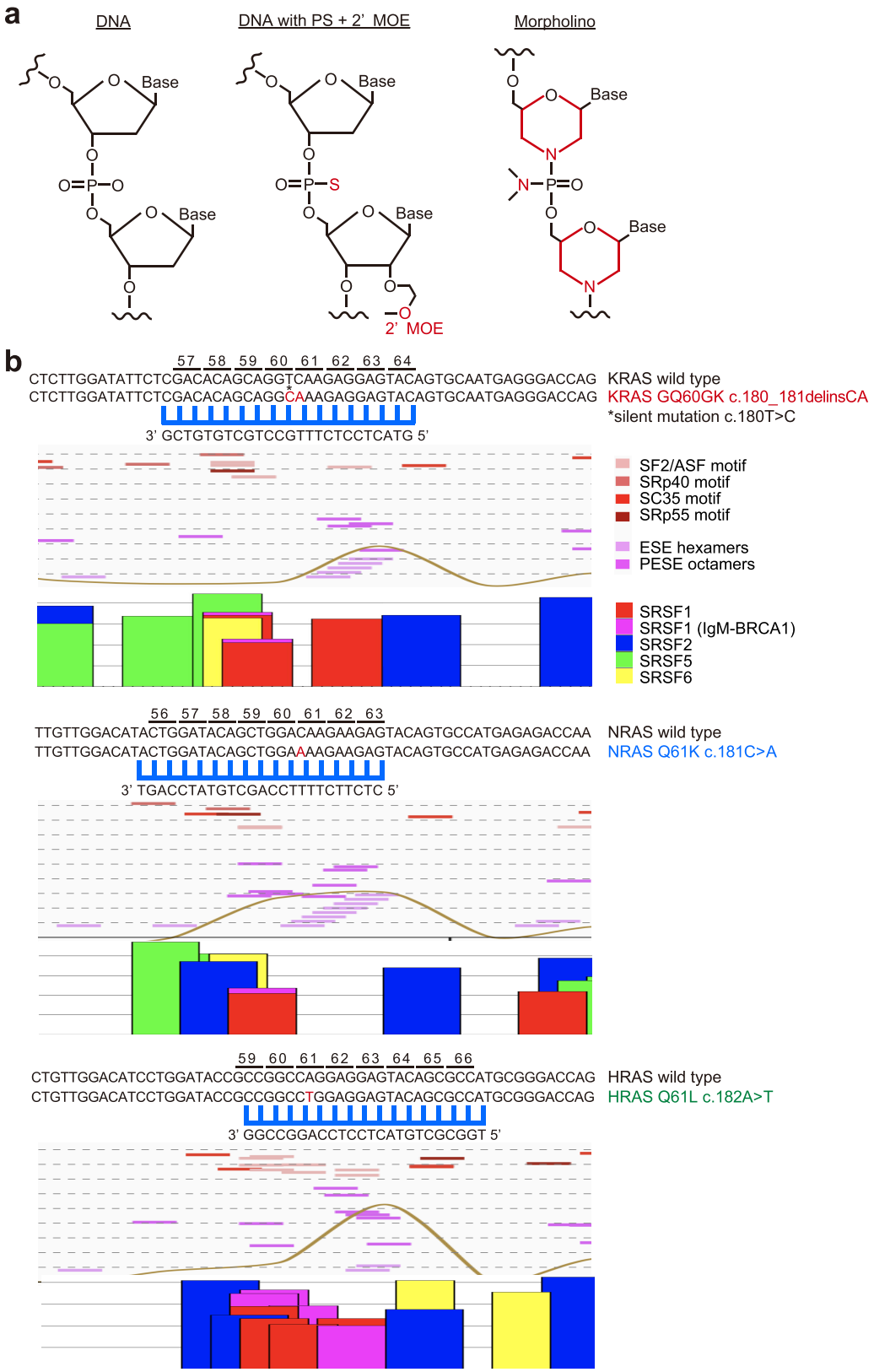

Extended Data Fig. 4 | Designing mutant-selective antisense oligos. **a**, Structures of DNA, antisense oligo nucleotides with phosphorothioate (PS) + 2'-O-Methoxyethyl (2'MOE) modifications, and morpholino. In PS+2'MOE, a non-bridging oxygen is replaced by a sulfur atom in the phosphate backbone, and 2' position of the sugar moiety is modified. In morpholino, the sugar moiety is replaced with methylenemorpholine rings, and the anionic phosphates are replaced with non-ionic phosphorodiamidate linkages. **b**, Schema depicting the design of the *KRAS* GQ60GK c.180_181delinsCA, *NRAS* Q61K, and *HRAS* Q61L selective antisense oligo. The motifs for binding exonic splicing enhancers simulated using the Human Splicing Finder (top) and ESE finder (bottom) are shown. Matrices for SR proteins including SRSF1 (SF2/ASF and IgM-BRCA1), SRSF2 (SC35), SRSF5 (SRp40), and SRSF6 (SRp55) are shown.

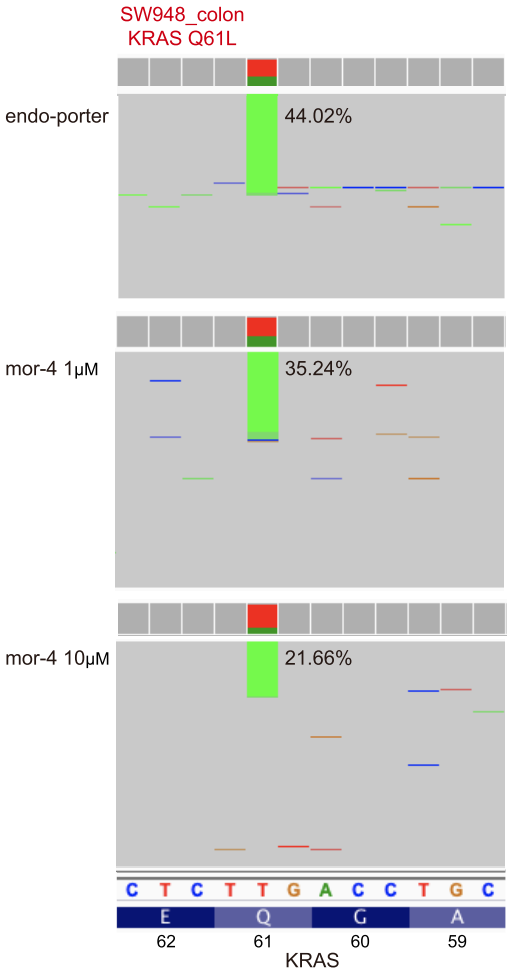

Extended Data Fig. 5 | Mutant selective inhibition of RAS using morpholino. Raw NGS reads showing *KRAS* Q61L transcript were visualized using IGV 2.8.0 software.

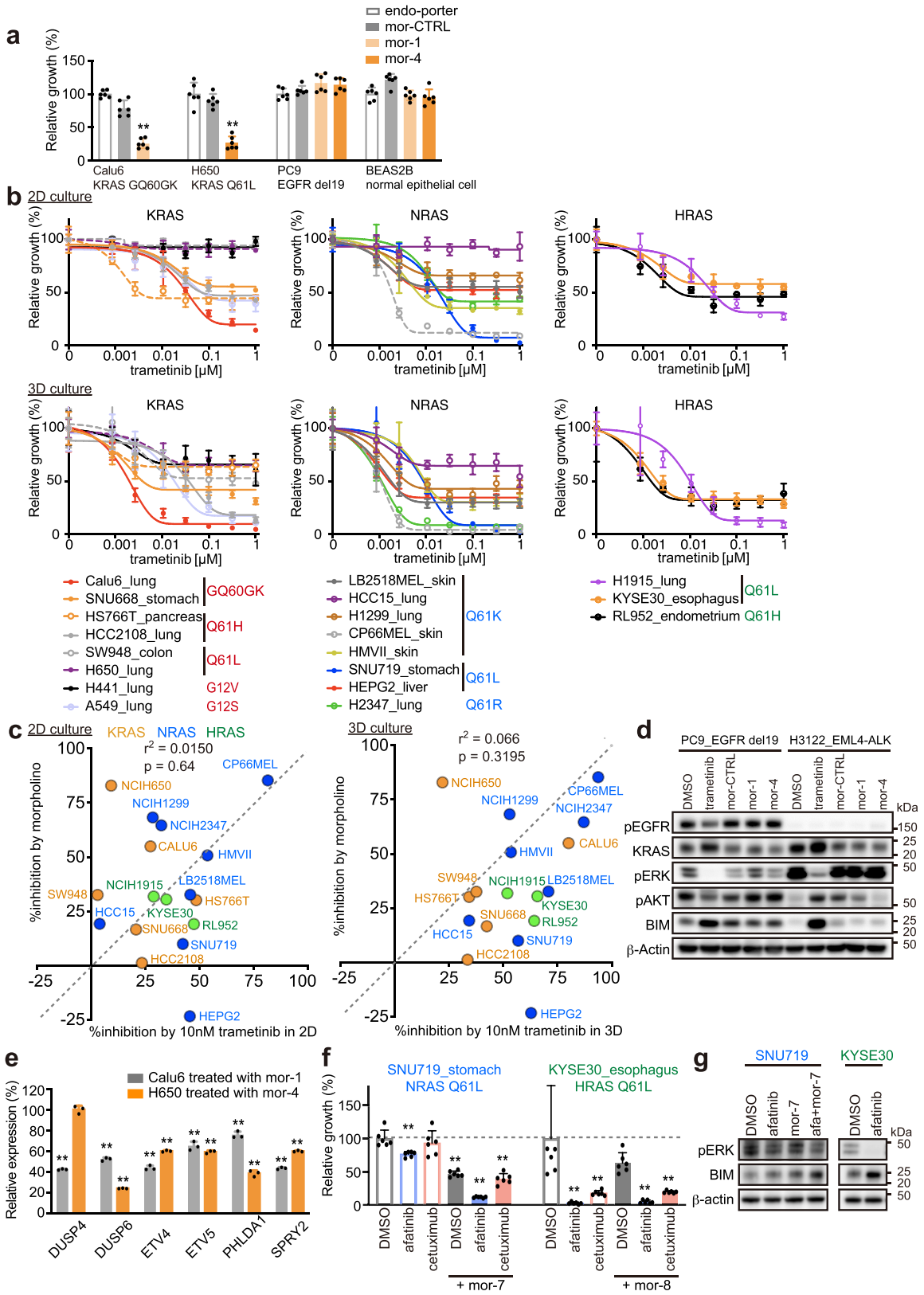

Extended Data Fig. 6 | See next page for caption.

Extended Data Fig. 6 | *In vitro* sensitivity to MEK inhibitor and morpholino oligos in *RAS* mutant cells. a. Cell viability assays of suspension cells after 8 days of 10 μM morpholino treatment were performed on ultra-low attachment plates (n = 6 biological replicates, mean ± s.d., ANOVA, followed by Dunnett's post-hoc test comparing to cells treated with DMSO, $^{**}p < 0.01$). **b**, Cell viability assay of a panel of mutant *RAS* cell lines after 72 h of trametinib treatment in 2D adherent or 3D suspension culture (n = 3 biological replicates, mean ± s.d.). **c**, The correlation of growth inhibition by 10 nM trametinib in 2D or 3D culture and morpholino antisense oligo nucleotide in 17 *RAS* Q61X cell lines. **d**, Western blot analyses of signaling in *KRAS* wild-type cell lines were performed after 72 h treatment with 10nM trametinib, 10 μM morpholino or respective controls. **e**, Relative expression of *ERK* signature genes, evaluated by qPCR in Calu6 and H650 cell lines treated with mutant-selective morpholino for 48 h. Expression data are normalized to readout of a control morpholino treatment. GUSB was used as an internal control. n = 3 biological replicates, mean ± s.d., t test, $^{**}p < 0.01$. **f**, Cell viability assays in suspension cells after 8 days of 50 nM afatinib, 10μg/ml cetuximub, and 10 μM morpholino treatment were performed with the same method as **a** (n = 6 biological replicates, mean ± s.d., ANOVA, followed by Dunnett's post-hoc test comparing to cells treated with DMSO, $^{**}p < 0.01$). **g**, Western blot analyses of signaling in *NRAS* and *HRAS* mutant cell lines were performed after 72 h of treatment with 10 nM trametinib, 10 μM morpholino, or DMSO.

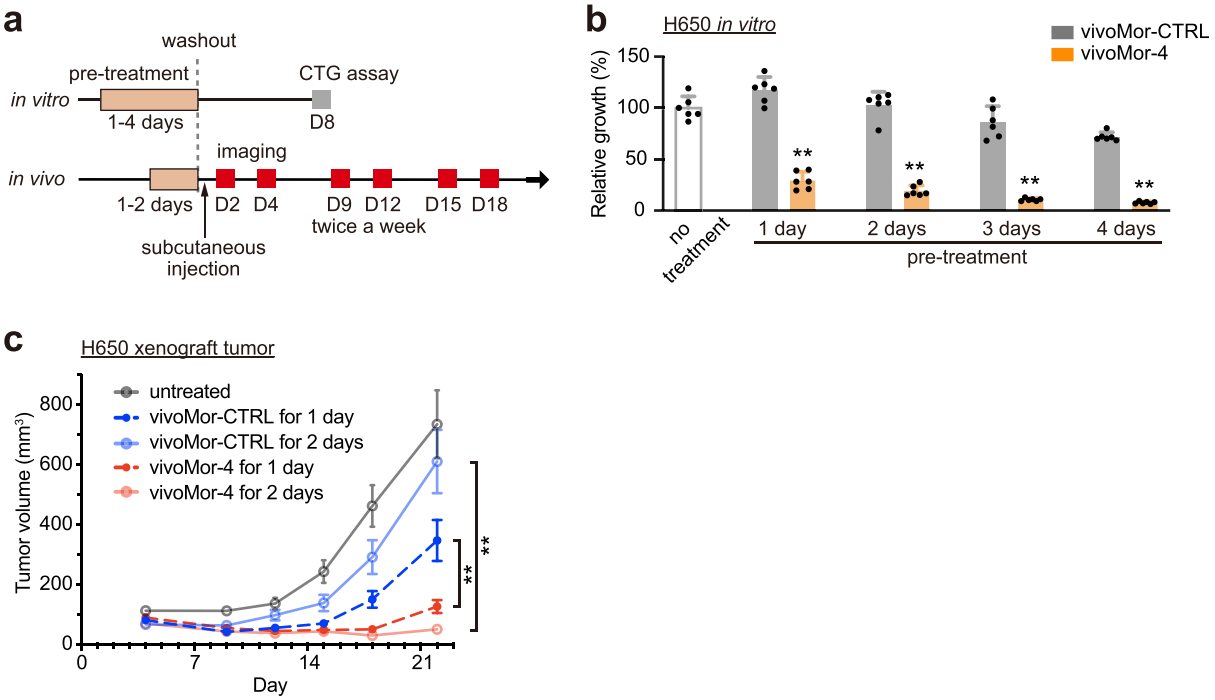

Extended Data Fig. 7 | Pre-treatment strategy using vivo-morpholino *in vitro* and *in vivo* H650 models. a, Morpholino oligo pre-treatment strategy. H650 cells were pre-treated with 10 µM control vivo-morpholino and target vivo-morpholino for 1 to 4 days as 3D suspension cells. After drug washout, cells were cultured in growth media and cell viability was evaluated on day 8 *in vitro*. Luciferase-expressing H650 cells were used for *in vivo* experiments. After pre-treatment with 10 µM vivoMor-CTRL and target vivo-morpholino for 1 to 2 days as 3D suspension cells, drugs were washed out and cells were subcutaneously implanted into mice. *In vivo* imaging was performed twice a week. **b**, *In vitro* cell viability assays of H650 cells pre-treated with 10µM vivoMor-CTRL or vivoMor-4 for 1 to 4 days (n = 6 biological replicates, mean ± s.d., t test, $^{**}p < 0.01$). **c**, Volume change of pre-treated H650 xenograft tumors. H650 cells were pre-treated with vivoMor-CTRL or vivoMor-4 *in vitro* for 1 or 2 days prior to injection into nude mice (n = 10 per each group, mean ± s.e.m., t-test and linear mixed growth models at day 22, $^{**}p < 0.01$).

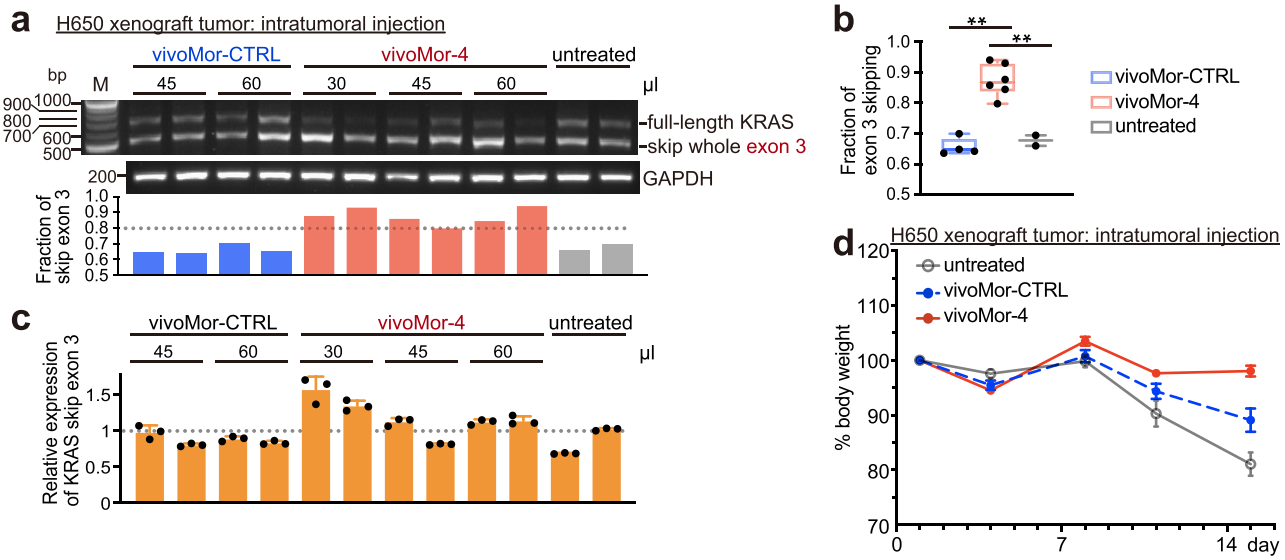

Extended Data Fig. 8 | Intra-tumoral injection of vivo-morpholino in H650 xenograft models. a, Images of KRAS-specific PCR amplicons generated from the cDNA of H650 xenograft tumors that were treated with daily intra-tumoral injection of morpholino for 7days. Fraction of exon 3 skipping is defined as the band intensities of "skipped/(skipped + full-length)" as measured by ImageJ (n = 1). M: 100 bp-marker. **b**, Fractions of exon 3 skipping in samples shown in (**a**) were compared using t test, **p < 0.01, n = 2–6 mice in each group, box plots show minimum, lower quartile, median, upper quartile, and maximum. **c**, Relative expression of KRAS exon 3 skipping, evaluated by qPCR in tumor samples corresponding to (**a**) (n = 3 biological replicates, mean ± s.e.m.). **d**, Body weight change of mice with H650 xenograft tumors treated with morpholino over time (n = 10 per each group, mean ± s.e.m.).

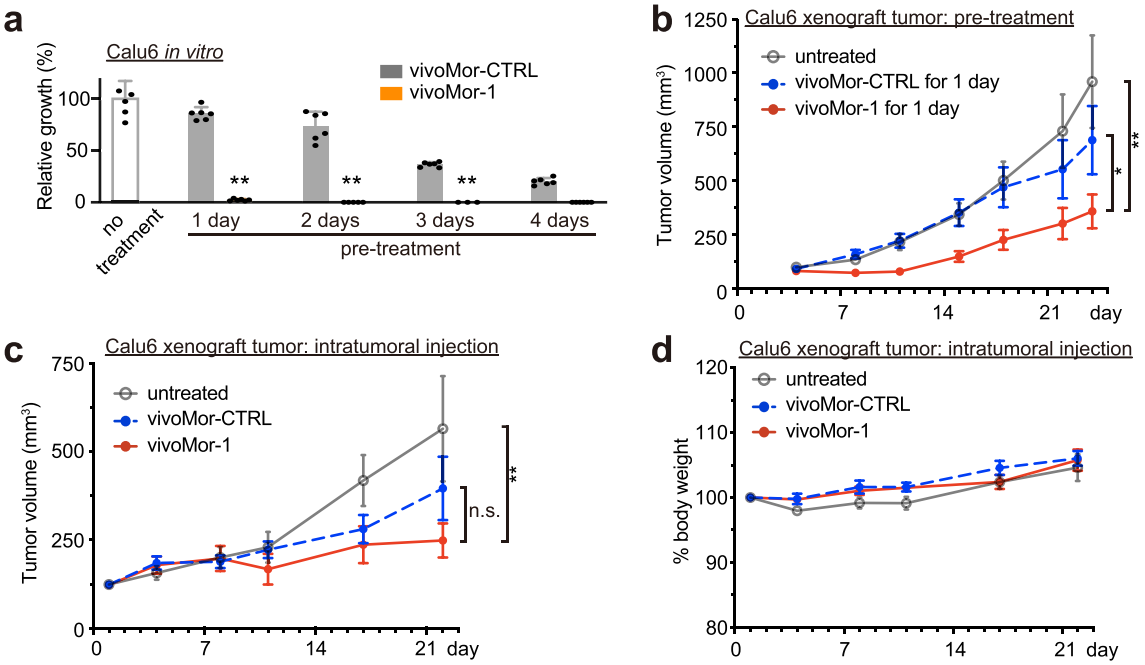

Extended Data Fig. 9 | Pre-treatment strategy and intra-tumoral injection of vivo-morpholino in Calu6 models. a, *In vitro* cell viability assays of Calu6 cells pre-treated with 10 µM vivoMor-CTRL or vivoMor-1 for 1 to 4 days (n = 6 biological replicates, mean ± s.d., t test, **p < 0.01). **b**, Volume change of pre-treated Calu6 xenograft tumors. Calu6 cells were pre-treated with vivoMor-CTRL or vivoMor-1 in vitro for 24 h prior to injection into nude mice (n = 10 per each group, mean ± s.e.m., t-test and linear mixed growth models, *p < 0.05, **p < 0.01). **c**, In vivo efficacy of Calu6 xenograft tumors treated with daily intra-tumoral injection of morpholino (n = 10 per each group, mean ± s.e.m., t-test and linear mixed growth models, **p < 0.01). **d**, Body weight change of mice with Calu6 xenograft tumors treated with morpholino over time (n = 10 per each group, mean ± s.e.m.).

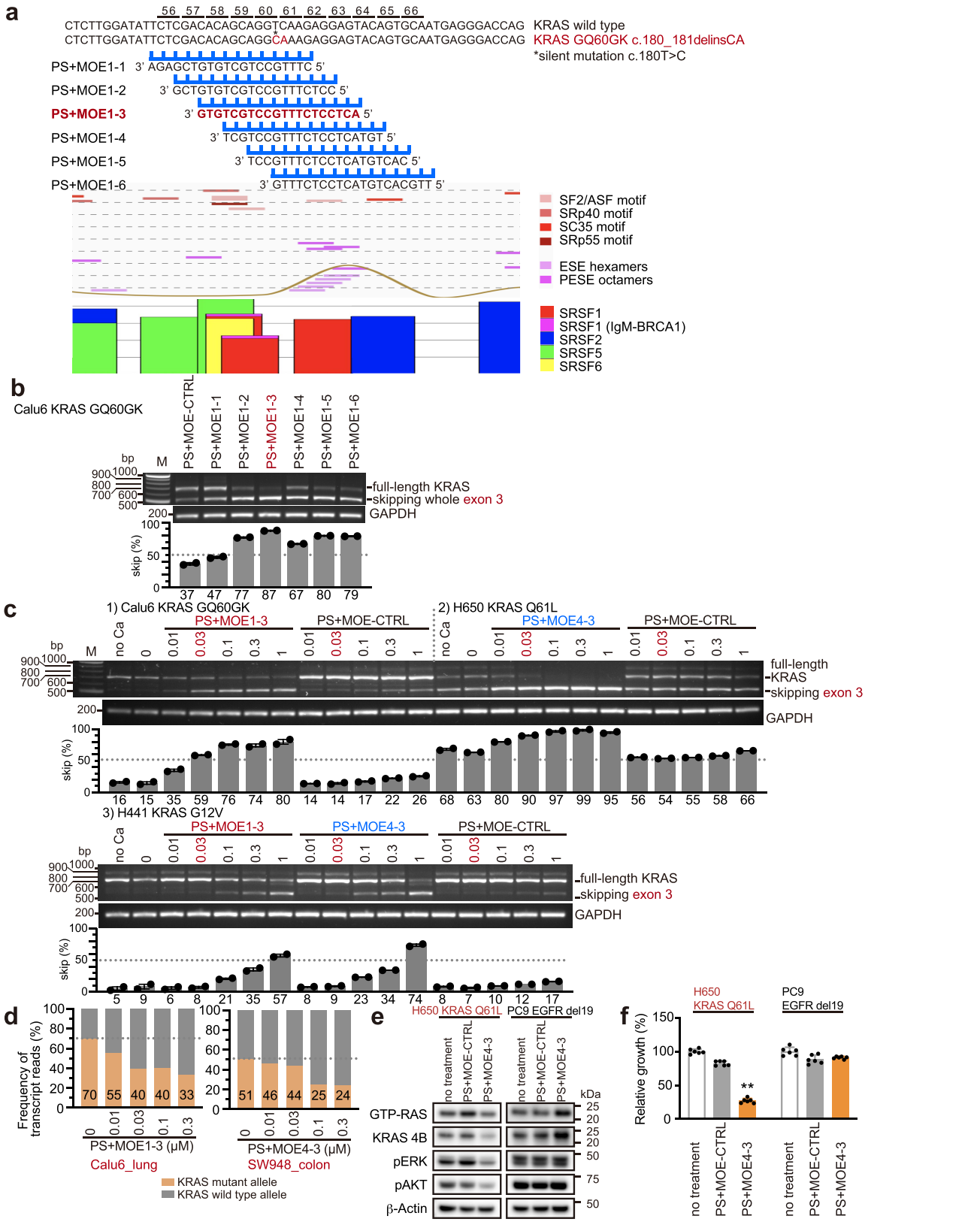

Extended Data Fig. 10 | Mutant selective inhibition of KRAS using PS+2′MOE antisense oligos. a, Schema depicting the design of the KRAS GQ60GK c.180_181delinsCA selective antisense oligo by screening. **b**, Images of KRAS-specific PCR amplicons generated from the cDNA of cells treated with 6 kinds of PS+2′MOE antisense oligos for 48 h. Exon 3 skipping fraction is defined as the band intensities of "skipped/(skipped + full-length)" transcript as quantified by ImageJ. M: 100 bp-marker. n = 2 biological replicates, mean ± s.e.m. **c**, Images of KRAS-specific PCR amplicons in indicated cell lines with same method as b (n = 2 biological replicates, mean ± s.e.m.). **d**, Transcript reads of KRAS GQ60GK or Q61L versus wild-type in the intact full-length KRAS amplicon derived from mRNA of Calu6 and SW948 cells treated with PS+2′MOE antisense oligos (n = 1). **e**, Western blot analyses of signaling in KRAS mutant and wild-type cell lines were performed after 6 days of 0.5 μM PS+2′MOE antisense oligos. **f**, Cell viability assays in suspension cells after 8 days of 0.5 μM PS+2′MOE antisense oligos treatment were performed (n = 6 biological replicates, mean ± s.d., t test, **p < 0.01).

nature research

Corresponding author(s): Yoshihisa Kobayashi and Pasi A. Jänne

Last updated by author(s): Dec 20, 2021

Reporting Summary

Nature Research wishes to improve the reproducibility of the work that we publish. This form provides structure for consistency and transparency in reporting. For further information on Nature Research policies, see our Editorial Policies and the Editorial Policy Checklist.

Statistics

For all statistical analyses, confirm that the following items are present in the figure legend, table legend, main text, or Methods section.

n/a	Confirmed	
☐	☒	The exact sample size (*n*) for each experimental group/condition, given as a discrete number and unit of measurement
☐	☒	A statement on whether measurements were taken from distinct samples or whether the same sample was measured repeatedly
☐	☒	The statistical test(s) used AND whether they are one- or two-sided *Only common tests should be described solely by name; describe more complex techniques in the Methods section.*
☐	☒	A description of all covariates tested
☐	☒	A description of any assumptions or corrections, such as tests of normality and adjustment for multiple comparisons
☐	☒	A full description of the statistical parameters including central tendency (e.g. means) or other basic estimates (e.g. regression coefficient) AND variation (e.g. standard deviation) or associated estimates of uncertainty (e.g. confidence intervals)
☐	☒	For null hypothesis testing, the test statistic (e.g. *F*, *t*, *r*) with confidence intervals, effect sizes, degrees of freedom and *P* value noted *Give P values as exact values whenever suitable.*
☒	☐	For Bayesian analysis, information on the choice of priors and Markov chain Monte Carlo settings
☒	☐	For hierarchical and complex designs, identification of the appropriate level for tests and full reporting of outcomes
☐	☒	Estimates of effect sizes (e.g. Cohen's *d*, Pearson's *r*), indicating how they were calculated

Our web collection on statistics for biologists contains articles on many of the points above.

Software and code

Policy information about availability of computer code

Data collection	EPSON perfection V750 pro (colony formation assay), BIO-RAD UNIVERSAL HOOD II Gel Documentation System with CFW-1312M Camera (images of PCR bands), StepOnePlus Real-Time PCR System (Quantitative RT-PCR data), FLUOstar Omega (Cell growth-inhibition assay), Amersham Imager 600 (Western blot), Perkin Elmer IVIS Spectrum (luciferase imaging)
Data analysis	SnapGene 4.1.9 (sequencing chromatogram), StepOne Software v2.3 (Quantitative RT-PCR), ImageQuant TL1D v8.2 (Western blot analysis), Perkin Elmer Living Image software v4.7.3 (luciferase imaging), GraphPad Prism v9.0.0, SAS 9.4, Adobe Photoshop v22.0.1, Adobe Illustrator 25.0.1, Human Splicing Finder v3.1 (splicing), ESE finder 3.0 (splicing), UNAFold Web Server (binding affinity), IGV 2.8.0 (visualizing NGS data)

For manuscripts utilizing custom algorithms or software that are central to the research but not yet described in published literature, software must be made available to editors and reviewers. We strongly encourage code deposition in a community repository (e.g. GitHub). See the Nature Research guidelines for submitting code & software for further information.

Data

Policy information about availability of data

All manuscripts must include a data availability statement. This statement should provide the following information, where applicable:

- Accession codes, unique identifiers, or web links for publicly available datasets
- A list of figures that have associated raw data
- A description of any restrictions on data availability

FASTQ files from the Amplicon sequencing of KRAS are available from the SRA database under BioProject accession number PRJNA789849. All data generated and Source Data are provided within the paper. Non-synonymous and silent mutations in KRAS, NRAS, and HRAS genes were obtained from TCGA pan-cancer cohort (https://portal.gdc.cancer.gov). Data on Exon 3 skipping at baseline in TCGA cohort were obtained from TCGA SpliceSeq (https://bioinformatics.mdanderson.org/public-software/tcgaspliceseq/). Gene effect scores for dependency, evaluated by RNAi and CRISPR knockout, were obtained from Depmap (https://depmap.org/

portal/).

Field-specific reporting

Please select the one below that is the best fit for your research. If you are not sure, read the appropriate sections before making your selection.

☒ Life sciences ☐ Behavioural & social sciences ☐ Ecological, evolutionary & environmental sciences

For a reference copy of the document with all sections, see nature.com/documents/nr-reporting-summary-flat.pdf

Life sciences study design

All studies must disclose on these points even when the disclosure is negative.

Sample size	A sample size of three to six replicates was selected for in vitro experiments, which were then confirmed via independent replication studies. Quantitative proteomics experiments were performed using n=2 biologically independent samples, which was expected to yield significant results based on previous experience. Each in vivo study had n=10 replicates per group to have appropriate statistical power based on previous experience.
Data exclusions	No data were excluded.
Replication	All experiments have been performed in at least two independent experiments. All replication attempts were successful.
Randomization	For in vitro experiments, wells of cells were randomly assigned to control or treatment groups. Mice bearing pre-treated H650 or Calu6 cells were not treated in vivo therefore, randomization was not required. In vivo study using intra-tumoral injection, mice with H650 or Calu6 xenograft models were randomized depending on the tumor size before treatment.
Blinding	Amplicon next generation sequencing was blinded. In vitro and in vivo experiments were not blinded; blinding was not applicable to this study as data collection and analysis was not prone to bias.

Reporting for specific materials, systems and methods

We require information from authors about some types of materials, experimental systems and methods used in many studies. Here, indicate whether each material, system or method listed is relevant to your study. If you are not sure if a list item applies to your research, read the appropriate section before selecting a response.

Materials & experimental systems

n/a	Involved in the study
☐	☒ Antibodies
☐	☒ Eukaryotic cell lines
☒	☐ Palaeontology and archaeology
☐	☒ Animals and other organisms
☒	☐ Human research participants
☒	☐ Clinical data
☒	☐ Dual use research of concern

Methods

n/a	Involved in the study
☒	☐ ChIP-seq
☒	☐ Flow cytometry
☒	☐ MRI-based neuroimaging

Antibodies

Antibodies used	All antibodies were described in Supplementary Table 10.
Validation	All antibodies are commercially available and the validation information found on suppliers' web page is as follows: p-EGFR (suitable for: WB, IHC, IF, FC; reacts with: human, mouse, rat, monkey; https://www.cellsignal.com/products/primary-antibodies/phospho-egf-receptor-tyr1068-d7a5-xp-rabbit-mab/3777); BRAF (suitable for: WB, IP, IF, IHC(P), ELISA; reacts with: mouse, rat, human; https://www.scbt.com/p/raf-b-antibody-f-7?productCanUrl=raf-b-antibody-f-7&_requestid=15560431); KRAS N-terminal (suitable for: WB, IP, IF, FC; reacts with: human, mouse, rat; https://www.ptglab.com/products/KRAS-Antibody-12063-1-AP.htm); KRAS 4B C-terminal (suitable for: WB, IHC, IF, FC; reacts with: human, mouse; https://www.ptglab.com/products/KRAS2B-speicifc-Antibody-16155-1-AP.htm); p-ERK (suitable for: WB, IP, IHC, IF, FC; reacts with: human, mouse, rat, hamster, monkey, mink, D. melanogaster, zebrafish, bovine, dog, pig, S. cerevisiae; https://www.cellsignal.com/products/primary-antibodies/phospho-p44-42-mapk-erk1-2-thr202-tyr204-d13-14-4e-xp-rabbit-mab/4370); t-ERK (suitable for: WB, IP, IHC, IF, FC; reacts with: human, mouse, rat, hamster, monkey, mink, D. melanogaster, zebrafish, bovine, dog, pig, S. cerevisiae; https://www.cellsignal.com/products/primary-antibodies/p44-42-mapk-erk1-2-137f5-rabbit-mab/4695); p-AKT (suitable for: WB, IP, IHC, IF, FC; reacts with: human, mouse, rat, hamster, monkey, D. melanogaster, zebrafish, bovine; https://www.cellsignal.com/products/primary-antibodies/phospho-akt-ser473-d9e-xp-rabbit-mab/4060), cleaved PARP (suitable for: WB, IP, IHC, IF, FC; reacts with: human, monkey; https://www.cellsignal.com/products/primary-antibodies/cleaved-parp-asp214-d64e10-xp-rabbit-mab/5625); BIM (suitable for: WB, IP, IHC, IF, FC; reacts with: human, mouse, rat; https://www.cellsignal.com/products/primary-antibodies/bim-c34c5-rabbit-mab/2933); b-actin (suitable for: WB; reacts

with: pig, Hirudo medicinalis, bovine, rat, canine, feline, human, rabbit, carp, mouse, guinea pig, chicken, sheep; https://www.sigmaaldrich.com/US/en/product/sigma/a3854); HSP90 (suitable for: WB, IP, IF, FC, ELISA; reacts with: mouse, rat, human: the vendor cites a paper showing detection of HSP90 by immunoblotting in human neuroblastoma cell lines PMID: # 20655465 Hölzel, M. et al. 2010. Cell. 142: 218-229; https://www.scbt.com/p/hsp-90alpha-beta-antibody-h-114?requestFrom=search), Active Ras Detection Kit (the vendor shows detection of RAS by immunoblotting in mouse NIH/3T3 cell lines; https://www.cellsignal.com/products/cellular-assay-kits/active-ras-detection-kit/8821).

Eukaryotic cell lines

Policy information about cell lines

Cell line source(s)	Sources of all cell lines were described in Supplementary Table 10.
Authentication	NCIH650, KYSE30, and RL952 cell lines were purchased specifically for this project from vendors listed in Supplementary Table 10 in December 2019 and used withing 10 passages. Other cell lines were originally purchased directly from the vendors listed in Supplementary Table 10, and then tested for mycoplasma contamination and STR fingerprinting. These cells were also used within 10 passages from the initially banked vials.
Mycoplasma contamination	All cell lines were periodically tested negative for Mycoplasma throughout the study.
Commonly misidentified lines (See ICLAC register)	None were misidentified.

Animals and other organisms

Policy information about studies involving animals; ARRIVE guidelines recommended for reporting animal research

Laboratory animals	7-week old female NSG mice (for H650 xenograft model) and NCr nude mice (for Calu-6 xenograft model) were purchased from The Jackson Laboratory. Animals were allowed to acclimate for at least 5 days before initiation of the study. Mice were housed in individually ventilated cages in a state-of-the-art OptiMICE rack system equipped with automatic watering. The vivarium was temperature controlled (72 ± 2° F) and a target range of 35-55% relative humidity, with automated lighting ensuring a standard 12:12 hour light/dark circadian cycle.
Wild animals	No wild animals were used in the study.
Field-collected samples	No field-collected samples were used in the study.
Ethics oversight	All in vivo studies were conducted at Dana-Farber Cancer Institute with the approval of the Institutional Animal Care and Use Committee in an AAALAC accredited vivarium.

Note that full information on the approval of the study protocol must also be provided in the manuscript.